Rap1 promotes epithelial integrity and cell viability in a growing tissue

C. Luke Messer and Jocelyn A. McDonald*

Division of Biology, Kansas State University, Manhattan, KS 66506

*Correspondence: jmcdona@ksu.edu

Running Title: Rap1 promotes epithelial integrity and cell survival

Abstract

Having intact epithelial tissues is critical for embryonic development and adult homeostasis. How epithelia respond to damaging insults or tissue growth while still maintaining intercellular connections and barrier integrity during development is poorly understood. The conserved small GTPase Rap1 is critical for establishing cell polarity and regulating cadherin-catenin cell junctions. Here, we identified a new role for Rap1 in maintaining epithelial integrity and tissue shape during *Drosophila* oogenesis. Loss of Rap1 activity disrupted the follicle cell epithelium and the shape of egg chambers during a period of major growth. Rap1 was required for proper E-Cadherin localization in the anterior epithelium and for epithelial cell survival. Both Myo-II and the adherens junction-cytoskeletal linker protein α-Catenin were required for normal egg chamber shape but did not strongly affect cell viability. Blocking the apoptotic cascade failed to rescue the cell shape defects caused by Rap1 inhibition. One consequence of increased cell death caused by Rap1 inhibition was the loss of polar cells and other follicle cells, which later in development led to fewer cells forming a migrating border cell cluster. Our results thus indicate dual roles for Rap1 in maintaining epithelia and cell survival in a growing tissue during development.

Introduction

Epithelia serve critical functions throughout the body's tissues and organs. For proper homeostasis, epithelia must remain as a cohesive unit while being amenable to essential remodeling events. This allows critical epithelial functions such as forming a barrier to pathogens, absorption of nutrients, wound healing, and other important roles (Abramson and Anderson, 2017; Blanpain and Fuchs, 2009; Bröer, 2008; Guillot and Lecuit, 2013; Tai et al., 2019). During development, many epithelial tissues undergo dramatic tissue rearrangements while staying intact, for example in convergent extension in *Drosophila* (Irvine and Wieschaus, 1994), ventral enclosure in *C. elegans* (Williams-Masson et al., 1997), and bottle cell invagination in *Xenopus* (Keller, 1981). Once formed, cells in epithelia must maintain polarized cell shapes, stay connected through cell-cell contacts, and survive insults imposed by the tissue environment. Epithelial tissues are challenged by cell turnover, cellular rearrangements, and apoptosis in response to normal tissue growth and homeostasis (Duszyc et al., 2017; Guillot and Lecuit, 2013). Because dysregulation of epithelia shape and cell survival can lead to diseases such as cancer, it is important to understand the mechanisms required for epithelial maintenance.

Here we report a requirement for the conserved small GTPase Rap1 in epithelial maintenance, where it contributes both to cell and tissue shape and to cell viability. The *Drosophila* ovary is an excellent model system to investigate how epithelial cells and tissues respond to challenges such as growth and shape changes during development. The ovary is made up of a series of continuously developing egg chambers. Each egg chamber consists of an inner population of germline derived cells enveloped in a continuous, polarized somatic cell epithelium made of follicle cells. Follicle cells continue to divide until stage 6, when mitosis ceases, resulting in a monolayer of ~650 cells. The follicle cells undergo a unique rotational migration that helps assemble a basement membrane layer. The basement membrane provides resistance to tissue growth and contributes to egg chamber shape (Duhart et al., 2017). The egg chamber starts out round but eventually grows and elongates to an ellipsoid shape starting in mid-oogenesis. During this process, the inner germline cells expand and press against the follicle cell layer, contributing to the characteristic ovoid shape of the egg. It is critical that the epithelium stays intact to allow successful oogenesis and proper development of a mature, fertilizable egg.

Rap1 plays key roles in epithelial morphogenesis during development, particularly in the establishment of tissue polarity and cell-cell adhesions. In *Drosophila*, Rap1 helps polarize epithelial cells by positioning Bazooka/Par3 (Bonello et al., 2018; Choi et al., 2013) and

promotes proper cell-cell adhesion by regulating E-Cadherin-rich adherens junctions (Knox and Brown, 2002). In human podocytes, as well as other cell types, Rap1 regulates integrin mediated adhesion to the basement membrane (Potla et al., 2014). Rap1 also promotes dynamic cell shape changes during development, including the elongation of cells at the leading edge of the lateral epidermis during *Drosophila* dorsal closure (Boettner et al., 2003; Boettner and Van Aelst, 2007).

Here we show that Rap1 GTPase maintains cell and epithelial shapes and promotes follicle cell survival during oogenesis. Loss of Rap1 altered the shape of follicle cells and the egg chamber itself. We find that Rap1 contributes to cell and tissue morphogenesis during mid-oogenesis by ensuring successful actomyosin contractility through α-Catenin/E-Cadherin adherens junctions in epithelial cells. Notably, inhibition of Rap1 also induced abnormal apoptosis of follicle cells. The pro-survival function of Rap1 was especially important in a specialized pair of epithelial follicle cells, the polar cells, during mid-oogenesis. When Rap1 was inhibited, polar cells failed to maintain the Death-associated inhibitor of apoptosis 1 (DIAP1), leading to loss of one or both polar cells. The loss of polar cells and other follicle cells subsequently led to fewer cells assembling into the migratory border cell cluster. Together, our results reveal dual roles for Rap1 in cell and epithelial morphogenesis and promoting cell viability within a developing tissue.

Results

Rap1 GTPase is required for proper egg chamber and epithelial shapes in mid-oogenesis

To better understand the role of Rap1 in epithelial maintenance, we first analyzed the localization of Rap1 using a functional GFP-Rap1 fusion protein expressed under the control of the endogenous *Rap1* promoter (Knox and Brown, 2002). Rap1 is expressed ubiquitously in all cells of the ovary, with highest enrichment at the apical cell cortex of all follicle cells (Fig. 1A-A'). The anterior polar cell pair has a particularly notable apical enrichment of GFP-Rap1, which resembles the patterns of the cell adhesion proteins E-cadherin and β-catenin (Armadillo/Arm) in the polar cells (Niewiadomska et al., 1999; Peifer et al., 1993). While Rap1 has known roles in the morphogenesis of diverse epithelia (Kim et al., 2022; Knox and Brown, 2002; Wang et al., 2013), few studies have analyzed how Rap1 maintains epithelia during tissue growth. To address this, we inhibited Rap1 activity in the follicle cells using a validated dominant negative Rap1 construct, UAS-DN-Rap1^{N17} (DN-Rap1^{N17}), whose expression results in phenotypes that strongly resemble loss of *Rap1* or Rap1 RNAi knockdown phenotypes in the embryo and ovary

(Boettner et al., 2003; Perez-Vale et al., 2022; Sawant et al., 2018). DN-Rap1^{N17} was driven by an epithelial-specific GAL4 driver, *c306*-GAL4 (Fig. 1B). Expression of *c306*-GAL4 begins early during oogenesis, but the highest expression occurs at mid-oogenesis (~stages 4-8) (Fig. 1B and Fig. S1A-B'). These stages coincide with a major egg chamber growth phase, that requires the follicular epithelium to stretch and challenges epithelial cell cohesion (Balaji et al., 2019; Crest et al., 2017; Haigo and Bilder, 2011; Spradling, 1993). Notably, *c306*-GAL4 is primarily expressed in anterior and posterior follicle cells, with mosaic or lower levels in central follicle cells (Fig. S1A', B').

The shape of egg chambers at stages 4-to-6 appeared to be normal in both control and DN-Rap1^{N17} egg chambers (Fig. 1C-D). However, by stages 7-8, the tissue shape of DN-Rap1^{N17}-expressing egg chambers was no longer normal, particularly at the anterior end (Fig. 1D). The anterior of DN-Rap1^{N17} egg chambers was wider compared to control (Fig. 1C-D). Closer inspection revealed altered anterior epithelial follicle cell shapes specifically in the *c306*-GAL4 expression region (Fig. 1B, D, F). DN-Rap1^{N17} follicle cells appeared to be stretched, rather than the expected cuboidal follicle cell shapes in control egg chambers at these stages (Fig. 1E, F). To determine if this phenotype was restricted to anterior follicle cells, we next used a pan-follicle cell driver *TJ*-GAL4, which is broadly expressed in all follicle cells by mid-oogenesis (Fig. S1C-D'; Hayashi et al., 2002). However, expression of DN-Rap1^{N17} driven by TJ-GAL4 caused wide-scale egg chamber degeneration, which precluded an assessment of either tissue or epithelial shapes (Fig. S1E-E').

Next, we further quantified the observed differences in anterior egg chamber shape, which we termed "local deformation". To do this, we measured the width of the anterior egg chamber at 20% of the total egg chamber length from the anterior end at stages 7-8 (*see* Materials and Methods; Fig. 1G, "in sheath"). Control egg chambers retained a characteristic "wedge" shape in this anterior region (mean of 37.49μm; Fig. 1G). DN-Rap1^{N17} inhibited egg chambers, however, were wider and more "cup" shaped (mean of 47.37μm; Fig. 1G, "in sheath"). These data together suggest that Rap1 promotes tissue and epithelial cell shapes during mid-oogenesis.

The shape of egg chambers, and potentially the follicular epithelium, could be influenced by the physical environment, such as packing of the egg chambers within the surrounding muscle sheath (also known as the "epithelial sheath"), position of egg chambers with respect to other ovarioles in the entire ovary, or even the position of the ovary within the abdomen itself (Andersen and Horne-Badovinac, 2016; Hudson et al., 2008; Schoborg et al., 2019; Valer et al., 2018). Therefore, we asked if the sheath was responsible for the observed egg chamber and

epithelial shape defects caused by inhibition of Rap1 (Fig. 1G, “in sheath” vs. “sheath removed”). We removed the muscle sheath prior to fixation in both control LacZ and DN-Rap1^{N17} and measured local deformation as before (Fig. 1G). In the case of control LacZ, egg chamber shape was the same whether the sheath was present (“in sheath”) or not (“sheath removed”; Fig. 1G). However, while DN-Rap1^{N17} inhibited egg chambers were locally deformed when the sheath was present, egg chamber shapes recovered to the control shape when the sheath was removed (Fig. 1G). The anterior epithelium of control LacZ egg chambers was smooth and regular at stage 8, both when egg chambers were fixed within the sheath (Fig. 1C, E) or fixed after the sheath was removed (Fig. 2A, 2B-B”, 2D). Notably, the anterior epithelium of DN-Rap1^{N17} inhibited egg chambers had irregular shapes, including thinning in places, both in the presence of sheath (Fig. 1D, F) and when the sheath was removed (Fig. 2C-C”, 2E). We also observed fewer follicle cells within the anterior region in DN-Rap1^{N17} inhibited egg chambers (mean 9.8 cells) compared to LacZ controls (mean 12.2 cells), consistent with the epithelium being more stretched in the absence of Rap1 (Fig. 2F). Finally, we measured apical-basal height of epithelial follicle cells found on either side of the polar cells (*see* Materials and Methods for details). Inhibition of Rap1 decreased overall cell height from a mean of 4.36μm in control to 3.66μm in DN-Rap1^{N17} (Fig. 2G), thus confirming a role for Rap1 in promoting normal epithelial cell shapes. Together, these data indicate that while the sheath can influence egg chamber shape, this occurs primarily when Rap1 is inhibited. Rap1 is required for epithelial cell shapes, which is not influenced by the muscle sheath. Therefore, we propose that Rap1 regulates the shape of the egg chamber and the shapes of anterior epithelial cells, potentially providing mechanical resistance to compression imposed by the surrounding muscle sheath.

Rap1 promotes polar cell shape and apical E-Cadherin accumulation

In addition to the overall distorted anterior follicular epithelial cell shapes in DN-Rap1^{N17} egg chambers, we observed particularly misshapen anterior polar cells compared to control (Fig. 1E, F; 3A-B”’). Polar cells are a specialized pair of follicle cells found at each pole of the egg chamber. Polar cells are one of the first specified follicle cells in the ovary and express unique cell markers such as the adhesion protein Fasciclin III (Fas III; Ruohola et al., 1991). Because the anterior egg chamber was most impacted by Rap1 inhibition, and GFP-Rap1 is highly enriched in polar cells, we focused on the function of Rap1 in the anterior polar cells.

Therefore, we next asked when and how polar cell shape was altered by loss of Rap1 activity. To do this, we quantified anterior polar cell shapes by defining their aspect ratio (AR).

We measured the width of each polar cell along their dorsoventral (DV) axis and divided by their length along the anterior-posterior (AP) axis (Fig. 3A-C). Control and DN-Rap1^{N17} polar cells at stages 4-6 were both typically longer along their AP axis than they were wide along the DV axis (AR=0.61 LacZ, AR=0.65 DN-Rap1^{N17}; Fig. 3C). At stages 7-8, control polar cells maintained the earlier ellipsoid shape, although they lengthened slightly along the AP axis (AR=0.56; Fig. 3A-A’’’, C). In contrast, DN-Rap1^{N17} polar cells at stages 7-8 frequently lost this elliptical shape and now extended along the DV axis, with more spherical shapes (AR=1.02; Fig. 3B-B’’’, C). Some Rap1-inhibited egg chambers also had more extreme cases of abnormal polar cell morphology. We observed examples in which one polar cell appeared to be missing (Fig. 3B-B’’’, S2A) or the polar cell pair was severely distorted into “dumbbell” type shapes (Fig. S2B). As described below, ~20% of late-staged egg chambers had fewer than two polar cells (e.g., Fig. 8C). However, defects in polar cell shapes occurred at stages 7-8 even when two polar cells were present (e.g., Fig. 1F, 2C”, 3C).

The defective polar cell shapes, combined with examples that appeared to split apart, prompted us to ask if polar cells in DN-Rap1^{N17} egg chambers were less adhesive. The homophilic cell-cell adhesion protein E-Cadherin accumulates at high levels in polar cells (Niewiadomska et al., 1999). E-Cadherin, as well as the associated cadherin-catenin complex member β-Catenin, highly localizes to the apical side of polar cells, particularly in the region where the polar cell pair is apically constricted (Niewiadomska et al., 1999; Peifer et al., 1993). Therefore, we next investigated if DN-Rap1^{N17} egg chambers accumulated E-Cadherin normally in polar cells (Fig. 4). We measured the apical E-Cadherin fluorescence intensity in egg chambers at stages 7-8 by drawing a line along the interface between polar cells, starting at the apical polar cell-polar cell contact (apical, “A”; Fig. 4A’, B’, C, D) and extending to the basal side (basal, “B”; Fig. 4A’, B’, C, D). In control egg chambers, we observed a higher peak in fluorescence signal intensity at the apical polar cell-polar cell interface compared to the basolateral surfaces (Fig. 4A-A”, C-D). Strikingly, in DN-Rap1^{N17} egg chambers the apical fluorescence enrichment was decreased and now resembled the fluorescence intensity along the lateral polar cell-polar cell interfaces (Fig. 4B-B”, C-D). To further assess E-Cadherin localization quantitatively, we determined the apicolateral intensity ratio by dividing the mean intensity of the portion of the line that corresponded to the apical contact by the mean intensity of the lateral region (Fig. 4E). Although the differences observed between LacZ controls and DN-Rap1^{N17} egg chambers did not reach statistical significance, the quantitation reveals a smaller mean value for DN-Rap1^{N17} (1.7) compared to the LacZ control (2.2) (Fig. 4E). Together, these findings suggest that Rap1 promotes the localized enrichment of E-Cadherin to

the apical interface between polar cells, which we propose regulates the normal shape of the polar cell pair.

Rap1 can regulate non-muscle myosin II (Myo-II) in some cellular contexts (Ando et al., 2013; Smutny et al., 2010). Therefore, we next asked if Rap1 regulated Myo-II in polar cells. Myo-II, as visualized with a functionally-tagged regulatory light chain, Spaghetti Squash-GFP, Sqh::GFP (Royou et al., 2004), is enriched across the entire apical surface of the anterior polar cell pair as well as other follicle cells (Fig. S3A-A'', C). However, we did not observe altered accumulation of Sqh:GFP fluorescence intensity at the apical surfaces of DN-Rap1^{N17} polar cells (Fig. S3B-B", C). Together, our results indicate that Rap1 is dispensable for accumulation of Myo-II but is required for E-Cadherin apical enrichment in polar cells at mid-oogenesis.

Myo-II and α-Catenin are required for egg chamber morphogenesis

Actomyosin contractility and adhesion both contribute to the shape and integrity of various tissues and organs during development (Harris and Tepass, 2010; Munjal and Lecuit, 2014). Therefore, we wanted to assess whether actomyosin contractility was required for local tissue morphogenesis similar to what we observed for Rap1 (Fig. 5A-E). We targeted the Myo-II regulatory light chain with RNAi-mediated knockdown (Sqh RNAi) and measured local (anterior) tissue deformation when the muscle sheath was present. Myo-II-deficient staged 7-8 egg chambers resembled what we observed in DN-Rap1^{N17} inhibited egg chambers within the sheath; the anterior tissue shape was wider and flatter than controls (compare Fig. 5B, E to Fig. 1D, G). These results were unexpected given that Rap1 inhibition did not affect apical Myo-II accumulation, at least in polar cells. Therefore, we reasoned that Rap1 may couple actomyosin contractility to the adherens junctions in the anterior epithelium, as has been described in other tissues (Sawyer et al., 2009).

To test this hypothesis, we next performed RNAi knockdown of E-Cadherin and α-Catenin, members of the adherens junction complex. E-Cadherin RNAi had no effect on egg chamber local deformation compared to GFP RNAi controls (Fig. 5A, C, E). The lack of observed phenotypes is likely due to known expression of N-cadherin in the follicular epithelium at these stages and compensatory upregulation of N-cadherin caused by loss of E-Cadherin (Loyer et al., 2015; Tanentzapf et al., 2000). Thus, we next knocked down α-Catenin (α-Cat), the linker protein that connects cadherin complex members to the cellular F-actin cytoskeleton (Wang et al., 2022; Yonemura et al., 2010). Downregulation of α-Catenin by RNAi resulted in a wider, locally deformed anterior egg chamber (Fig. 5D, E), resembling the tissue shape defects

observed with Sqh RNAi and DN-Rap1^{N17} (Fig. 5B, E; Fig. 1D, G). Thus, adhesion and actomyosin are required to maintain tissue shapes at mid-oogenesis.

We next examined the shape of epithelial follicle cells at the anterior end of the egg chamber when Myo-II or α-Catenin were knocked down by RNAi (Fig. 5F-I'). Closer inspection revealed altered individual cell shapes resembling those in DN-Rap1^{N17} egg chambers, particularly for α-Catenin RNAi (Fig. 5 H-I'). Notably, we observed a mix of "stretched" or "flattened" follicle cells in α-Catenin RNAi egg chambers along the lateral sides of the egg chamber that resembled the cells in the anterior region of DN-Rap1^{N17} egg chambers (Fig. 5H-I'; compare to Fig. 1F and 2C-C"). In the most-affected α-Catenin RNAi egg chambers (Fig. 5I, I'), severe epithelial stretching was observed, which closely resembled the cell shape defects reported for *α-Catenin* null mutant follicle cells (Sarpal et al., 2012). Further supporting this, previous work by Tanentzapf and colleagues showed that loss of β-catenin at these stages also disrupts the normal follicle cell architecture, resulting in irregular thinning of the epithelium (Tanentzapf et al., 2000). The similarities in the tissue and epithelial cell shape phenotypes caused by loss of α-Catenin and Rap1 activity thus suggests that Rap1 modulates α-Catenin-containing adherens junctions as was observed during dorsal fold formation in the *Drosophila* embryo (Wang et al., 2013).

Rap1 promotes the viability of epithelial follicle cells during oogenesis

Our analysis of DN-Rap1^{N17} egg chambers at stages 7-8 revealed not only cases of distorted polar cell shapes, but also examples in which one polar cell was missing from the required pair (Fig. 3B-B"', S2A). These data suggested that Rap1 may contribute to cell survival. To test this idea, we first analyzed apoptosis during oogenesis in control and Rap1 mutant ovaries (Fig. 6). We stained egg chambers for an antibody that recognizes cleaved death caspase-1 (cDcp-1), which recognizes both *Drosophila* effector caspases, Death caspase-1 (Dcp-1) and Death related ICE-like caspase (Drice) (Li et al., 2019; Vasudevan and Ryoo, 2016). During early oogenesis, excess polar cells ("supernumerary" polar cells) and excess stalk cells form but are eliminated by apoptosis during stages 3-6, whereas in healthy ovarioles other follicle cells do not undergo cell death (Borensztejn et al., 2018, 2013; Khammari et al., 2011; Lebo and McCall, 2021) (cDCp-1+ cells; Fig. 6A-A'). However, in DN-Rap1^{N17} ovarioles, in addition to the normal pattern of early polar cell and stalk cell apoptosis, we observed additional caspase activity in follicle cells during stages 2 through 8 of oogenesis (cDCp-1+ cells; Fig. 6B-B'). We further quantified the number of cDcp-1+ cells grouped by egg chamber stage in control and DN-Rap1^{N17} ovarioles (Fig. 6F). We observed a significant increase in apoptotic cells when Rap1

activity was inhibited, particularly between stages 3-6 (Fig. 6F). Increased activation of Rap1, through expression of constitutively active CA-Rap1^{V12}, did not decrease the number of apoptotic cells during any stage of oogenesis compared to lacZ control (Fig. 6F). These data suggest that Rap1 is required for follicle cell survival during oogenesis but is not sufficient to block normal developmental apoptosis.

Because Rap1 promotes both follicle cell survival and epithelial and tissue morphogenesis during oogenesis, we next asked if Myo-II or α-Catenin were also similarly required for follicle cell viability. We analyzed cell death during oogenesis by cDcp-1 staining of Sqh RNAi, α-Catenin RNAi, and matched control (GFP RNAi) ovarioles. We observed a mild increase in cell death at some stages of oogenesis for both Sqh RNAi and α-Catenin RNAi as compared to GFP RNAi controls (Fig. 6C-E', G). These results suggest that both Myo-II and α-Catenin regulate egg chamber morphogenesis but have minor roles in follicle cell viability.

Rap1 promotes polar cell survival by suppressing apoptosis

Rap1 promotes both cell survival and tissue morphogenesis, whereas Myo-II and a-Catenin mainly function in tissue and cell shape. Therefore, we wanted to determine if Rap1 more directly contributes to cell viability. We focused on the polar cells, both because Rap1 promotes their normal shape (Figs. 3 and S2) and because polar cells play important roles in oogenesis (Duhart et al., 2017; Grammont and Irvine, 2002). Normal polar cell apoptosis occurs during stages 2-6, resulting in a "mature" polar cell pair by stages 7-8 (Fig. 6F; Borensztejn et al., 2013; Khammari et al., 2011). We tracked accumulation of cDcp-1 in mature polar cells at stages 7-8 (Fig. 7A-B"'). Control mature polar cells rarely died at these stages (Fig. 7A-A"';1 out of 66 egg chambers). In contrast, we observed an increased frequency in the accumulation of cDcp-1 in staged 7-8 DN-Rap1^{N17} polar cells, well after the conclusion of normal developmental apoptosis (Fig. 7B-B"'; 7 out of 61 egg chambers). The cDcp-1+ polar cells were frequently pyknotic as visualized by DAPI staining (Fig. 7B'-B"). These data indicate that Rap1 promotes the survival of mature polar cells during oogenesis, in addition to other follicle cells (Fig. 6B, B', F).

To further characterize why Rap1 promotes mature polar cell viability, we next examined the apoptotic cascade. Death-associated inhibitor of apoptosis 1 (DIAP1) blocks caspase activity and thus prevents cells from undergoing apoptosis (Hay et al., 1995; Yan et al., 2004). DIAP1 is specifically downregulated in "supernumerary polar cells" that undergo developmental apoptosis but accumulates in the two polar cells that will survive (Borensztejn et al., 2013; Khammari et al., 2011). We reasoned that a decrease in DIAP1 might precede the death of mature polar cells observed in DN-Rap1^{N17} egg chambers. Therefore, we analyzed DIAP1

accumulation in polar cells relative to their most adjacent follicle cell neighbors at stages 4 to 6 prior to the global downregulation of DIAP1 that occurs at stage 7 to 8 of oogenesis (Baum et al., 2007). At stages 4-6, we observed normal accumulation of DIAP1 in 13 out of 14 control polar cell pairs (Fig. 7C-C"). In contrast, DIAP1 accumulated in only 6 out of 23 DN-Rap1^{N17} polar cell pairs (Fig. 7D-D"). Interestingly, DIAP1 levels were altered at a greater frequency in DN-Rap1^{N17} egg chambers (Fig. 7D-D") than the observed frequency of polar cell death (Fig. 7B"'). One possibility is that not all cells that lose DIAP1 accumulation undergo cell death. Alternatively, the threshold for DIAP1 protein depletion may need to be relatively severe for apoptosis to occur. Taken together, our results favor a role for Rap1 in suppressing the apoptotic cascade through regulating the levels of DIAP1 in mature polar cells.

We next asked if the polar cell morphology defects caused by loss of Rap1 activity were due to apoptosis. To test this, we asked if blocking the apoptotic cascade could rescue the polar cell shape defects caused by loss of Rap1 activity (Fig. 3B-C; Fig. S4A). We performed polar cell aspect ratio measurements in egg chambers that co-expressed DN-Rap1^{N17} with either a LacZ control or with baculoviral p35, a strong inhibitor of apoptosis (Clem et al., 1991; Hay et al., 1994). We found that co-expression of p35 along with DN-Rap1^{N17} failed to rescue the polar cell aspect ratio defects compared to co-expression with LacZ (Fig. S4B-C). There was no statistical difference in the aspect ratios of DN-Rap1^{N17} polar cells when co-expressed with the LacZ control or with p35 (AR=0.84, DN-Rap1^{N17} + LacZ; AR=0.85, DN-Rap1^{N17} + p35; Fig. S4C). These results support a model in which Rap1 controls polar cell morphogenesis independently of its function in promoting cell survival.

Rap1 requirement for cell survival supports formation of border cell clusters with optimal cell numbers

The role for Rap1 in promoting polar cell survival prompted us to next ask what the developmental consequences were later in oogenesis. During late stage 8, the anterior pair of polar cells specifies which follicle cell neighbors become the migratory border cells through the secretion of the JAK/STAT ligand Unpaired (Beccari et al., 2002; Silver and Montell, 2001). Between 4-to-8 follicle cells with the highest levels of active JAK/STAT are then subsequently recruited to surround the polar cell pair, thus producing a border cell cluster with a total of 6-to-10 cells (Silver and Montell, 2001). Having an optimal number of cells helps the border cell cluster efficiently reach the oocyte at the correct time (Cai et al., 2016; Starz-Gaiano et al., 2008; Stonko et al., 2015).

Because inhibition of Rap1 caused a frequent loss of mature polar cells, we thus asked how this impacted the migratory border cell cluster. We first quantified the total number of cells found within control (LacZ) versus Rap1-deficient (DN-Rap1^{N17} or Rap1 RNAi) border cell clusters (Fig. S5A-C). When Rap1 was inhibited by *c306*-GAL4 driving DN-Rap1^{N17}, the average number of cells per cluster was significantly reduced compared to control clusters (Fig. S5A-C; average of 6.1 cells in control LacZ; average of 4.6 cells in DN-Rap1^{N17}). In *c306*-GAL4-driven *Rap1* RNAi egg chambers, the number of cells per cluster was also reduced compared to control (Fig. S5C; average of 6.1 cells in *mCherry* RNAi control; average of 5.2 cells in *Rap1* RNAi). Since the migratory cluster is composed of both border cells and polar cells, we next asked how cell composition was impacted. We observed border cell clusters missing one or both polar cells in 20% of DN-Rap1^{N17} border cell clusters compared to 6.9% of control clusters (Fig. 8A-C). These results agree with the earlier polar cell survival defects found in DN-Rap1^{N17} egg chambers (Fig. 7B-B'''). Strikingly, however, we observed a decrease in the total cells per cluster, both in all clusters (whether missing a polar cell or not) and those that had two polar cells present (Fig. 8D-E). We also observed significant border cell migration defects for Rap1 inhibited egg chambers as compared to controls (Fig. 8F-H), in agreement with previous studies (Chang et al., 2018; Sawant et al., 2018). Notably, however, overall egg chamber health appeared normal using this GAL4 driver (Fig. 8I). Although we occasionally observed degenerating egg chambers (e.g., Fig. 6B, B'), the frequency of degenerating egg chambers in *c306*-GAL4 Rap1-inhibited tissues was comparable to that of LacZ controls (Fig. 8I). However, global downregulation of Rap1 (Asha et al., 1999) or expression of DN-Rap1^{N17} in all follicle cells (Fig. S1E, E') caused an increase in egg chamber degeneration, suggesting that Rap1 does play a role in egg chamber health.

We also analyzed the number of cells in border cell clusters using a different GAL4, *slbo*-GAL4, which is expressed later than *c306*-GAL4 and in a more restricted pattern (Fig. S6A). The overall number of cells in *slbo*-GAL4 control egg chambers was higher than that observed for *c306*-GAL4 controls (average of 8.2 cells; Fig. S6B, B', D). We observed a significant reduction in the number of cells within the border cell cluster for DN-Rap1^{N17} expressing egg chambers (Fig. S6C-D; average 6.7 cells). The differences in cell numbers found in *c306*-GAL4 versus *slbo*-GAL4 may be due to genetic backgrounds or the distinct spatial-temporal expression patterns of each GAL4. Nonetheless, our data support a role for Rap1 in promoting cell survival and/or incorporation of the optimal number of cells into the border cell cluster.

We next asked if the observed reduction in cell numbers within the border cell cluster was due to a requirement for Rap1 to specify border cells. We examined anterior follicle cells at stage 8 for a reporter of JAK/STAT activity, 10XSTAT::GFP (Bach et al., 2007). The 10XSTAT::GFP+ cells are fated to become migratory border cells (Beccari et al., 2002; Silver and Montell, 2001). When both polar cells were present, we did not detect changes in either the pattern of 10XSTAT:GFP or the levels of nuclear STAT, and hence activity, in the three follicle cells immediately adjacent to the polar cells at stage 8 in *c306*-GAL4-driven DN-Rap1^{N17} compared to control LacZ egg chambers (Fig. S7A-C). These results suggest that border cell fate specification at stage 8 of oogenesis is normal under conditions when both polar cells are present and does not rely on Rap1 activity. However, we cannot rule out a subtle decrease in the JAK/STAT activity gradient when only one polar cell survives to stage 8 in DN-Rap1^{N17} egg chambers.

Finally, we asked if the smaller number of cells per border cell cluster was due to the increased apoptotic activity observed upon Rap1 inhibition. We co-expressed DN-Rap1^{N17} with either a UAS-LacZ control or the apoptosis inhibitor UAS-p35 (Fig. 9A-B', E). Border cell clusters that co-expressed DN-Rap1^{N17} and LacZ had an average of 4.7 cells per cluster, resembling the phenotypes observed when expressing DN-Rap1^{N17} alone (compare Fig. 9A, A', E to Fig. 8B, D and Fig. S5B-C). In contrast, border cell clusters co-expressing DN-Rap1^{N17} and p35 had an average of 6.3 cells per cluster (Fig. 9B, B', E), resembling what was observed in LacZ control border cell clusters (Fig. 8A, A', D). Thus, p35 inhibition of apoptosis restored total cell number in DN-Rap1^{N17} border cell clusters. Expression of p35 likely promotes polar cell survival and inclusion in migratory clusters. In support of this, addition of p35 suppressed the loss of polar cells observed in DN-Rap1^{N17} + LacZ clusters (Fig. 9C). Moreover, clusters co-expressing DN-Rap1^{N17} + p35 had extra polar cells, which may account for the increased number of cells found in border cell clusters (Fig. 9D, E). Supporting this idea, DN-Rap1^{N17} border cell clusters with only 2 polar cells had similar numbers of cells whether p35 was expressed or not (Fig. 9F). These results were not specific to DN-Rap1^{N17}, as expression of p35 in combination with LacZ was sufficient to promote survival of extra polar cells in 38.9% of border cell clusters (Fig. 9H, H', I), whereas expression of LacZ resulted in extra polar cells in only 5.6% of clusters (Fig. 9G, G', I). Expression of p35 resulted in more cells per border cell cluster, but only when more polar cells were present (Fig. 9J); p35 + LacZ clusters with two polar cells had similar number of cells as control LacZ clusters (Fig. 9K). The most likely interpretation is that p35 expression, with or without DN-Rap1^{N17}, causes early excess polar cells to survive to late stages, rather than undergo their normal developmental apoptosis

(Borensztejn et al., 2013; Khammari et al., 2011). These data thus suggest that the reduction in cell number per cluster caused by Rap1-inhibition is at least partly due to the death of the mature polar cells just prior to recruitment of border cells (Figs. 8, 9) but is independent of border cell specification (Fig. S7). Additionally, Rap1 may promote the survival of follicle cells that become border cells or inclusion of presumptive border cells within the migratory cluster (Fig. 8E). Thus, we propose a model in which Rap1 promotes mature polar cell survival by preventing apoptosis through upregulation of DIAP1, as well as other follicle cells, thus promoting an optimal number of cells being recruited to form the migrating border cell cluster.

Discussion

A key challenge is to understand how epithelia and constituent cells survive and maintain shape in response to the changes in tissue shape and size during normal development. Here we focused on understanding how the small GTPase Rap1 maintains cell and tissue shapes during *Drosophila* egg chamber growth. Prior work has shown requirements for Rap1 in epithelial morphogenesis (Asha et al., 1999; Boettner and Van Aelst, 2007; Bonello et al., 2018; Choi et al., 2013), but whether and how Rap1 maintains the epithelium during tissue growth and homeostasis was unclear. Here we used a model of developmental tissue growth in the *Drosophila* ovary to interrogate the function of Rap1. We found that Rap1 promotes the shapes of epithelial follicle cells, polar cells, and the local tissue during a period of major egg chamber growth. We propose that this function of Rap1 in maintenance of epithelial integrity is through regulation of dynamic linkages between adherens junctions and the contractile actomyosin cytoskeleton. This in turn may help egg chambers resist mechanical compression by the overlying muscle sheath to allow proper packing of egg chambers into each ovariole and bundling of ovarioles into the entire ovary. Our experiments revealed an unexpected and new role for Rap1 in regulating follicle cell survival, especially of the mature polar cells, which leads to the assembly of migratory border cell clusters with the optimal number of cells.

Rap1 maintains cell and tissue shapes by modulating adherens junction-cytoskeleton linkages during tissue growth

Here we report that Rap1 is required to maintain polar cell and follicle cell shapes and proper tissue shapes of the anterior follicular epithelium during egg chamber elongation. Our quantitative analyses of individual cell shapes and local tissue deformation demonstrated that Rap1 maintained tissue and epithelial morphology. Moreover, the shapes of Rap1-deficient follicle cells and polar cells were greatly affected. Most of these phenotypes were observed at

stages 7-8, a period of dramatic egg chamber growth (Crest et al., 2017). Previous work using *Rap1* null flies that were rescued to viable adults by expression of heat shock-driven Rap1 revealed egg chambers that degenerated at mid-to-late stages of oogenesis (Asha et al., 1999). Notably, prior to degeneration, egg chambers had distorted follicle cell shapes and discontinuities (Asha et al., 1999). Supporting a role for Rap1 in tissue maintenance, we obtained similar, albeit less severe egg chamber defects, by specifically expressing DN-Rap1^{N17} in anterior follicle cells. We also found that Rap1 maintains tissue shape when the muscle sheath is present. These results indicate a requirement of Rap1 in tissue shape maintenance.

How does Rap1 contribute to cell and tissue shape maintenance within the follicular epithelium during tissue expansion? Rap1 regulates early Bazooka/Par3 localization and adherens junction positioning during *Drosophila* embryogenesis (Bonello et al., 2018). *Rap1* mutant embryos fail to localize spot adherens junctions properly during cellularization and complete embryogenesis with fragmented cuticles suggesting a loss of tissue integrity (Choi et al., 2013). Similarly, Rap GTPase family proteins are required for adherens junctions and tight junction formation in MDCK cells (Sasaki et al., 2020). Our results showed that Rap1 is required specifically for the enrichment of E-Cadherin at the apical side of polar cells, which we propose helps promote proper polar cell shapes. We also observed stretching of the anterior epithelial follicle cells, which may indicate altered adhesion in these cells. Importantly, epithelial defects occurred whether the muscle sheath was present or not. E-cadherin appeared to be localized to apical puncta between follicle cells consistent with the formation of adherens junctions. However, these junctions may not be completely normal, which may contribute to the observed stretched and compressed epithelial shapes upon Rap1 inhibition. We propose that Rap1 maintains (or helps assemble) the proper positioning of the apical adherens junction in polar cells; further work will be needed to determine if and how Rap1 mechanistically maintains adherens junctions in the follicle cells.

The functions of adherens junctions in maintaining cell-to-cell contacts within an epithelium are also coupled to actomyosin contractility, which can drive cell shape changes. Rap1 and its effector Canoe (Cno) regulate actomyosin contractility in apically constricting mesodermal cells during *Drosophila* ventral furrow invagination (Sawyer et al., 2009; Spahn et al., 2012). Similarly, Rap1 is required for Shroom-dependent apical constriction in *Xenopus* (Haigo et al., 2003). These studies led us to ask if, in addition to its role in positioning adherens junctions during egg chamber elongation, Rap1 was responsible for proper actomyosin contractility. We found that Myo-II was required for proper tissue shape during egg chamber elongation, but surprisingly Rap1 was dispensable for Myo-II localization in polar cells. Taken

together with the stretched individual cell shapes and deformed egg chambers observed for α-Catenin RNAi, these data support our model that Rap1 maintains the strength of adherens junction-actin linkages as was reported for Cno (Sawyer et al., 2009).

We found that Rap1 regulates egg chamber and cell shapes during a period of major tissue growth. The inherent on-off activity states of GTPases like Rap1 make them particularly useful for dynamic processes that require discrete bursts of activity in response to cellular or tissue level cues (Gloerich and Bos, 2011). In apical constriction, for example, myosin pulsatility is coupled to progressive tightening of the apical domain (Martin et al., 2009; Martin and Goldstein, 2014). The transient nature of pulsatile myosin may require a fast-acting molecular switch that can be activated and inactivated quickly to couple motor behaviors to changes at the cell cortex. While we did not observe Myo-II localization defects when Rap1 was inhibited, the requirement for α-Catenin indicates that linkage to the actomyosin cytoskeleton is critical for epithelial cell and tissue shapes. Atypical Protein Kinase C (aPKC) promotes an optimal level of actomyosin to maintain an intact and organized follicle cell epithelium (Osswald et al., 2022). Indeed, acute loss of aPKC causes the follicle cell layer to apically constrict and rupture, due to growth of the egg chamber. Loss of Rap1 activity did not cause the epithelium to rupture; instead, the tissue locally deformed. Tissue shape depended on presence of the muscle sheath, but only in Rap1-inhibited egg chambers, suggesting that Rap1 helps the egg chamber resist mechanical compression. The basement membrane becomes thinner at the anterior and posterior ends during tissue elongation, allowing further growth along the anterior-posterior axis (Balaji et al., 2019; Crest et al., 2017). We suggest that loss of Rap1, in conjunction with a permissive region of the basement membrane, allows the tissue to widen in response to egg chamber growth and packing of egg chambers imposed by the muscle sheath. While there may be specific roles for Rap1 at the anterior pole, we cannot yet rule out more general Rap1 functions in the rest of the epithelium. Thus, we propose that Rap1, through apical enrichment of adherens junction proteins, reinforces strong epithelial connections and resistance to growth of the germline and compression by the overlying muscle sheath.

The signal relay mechanisms that act upstream to regulate the various Rap1 activities in the follicle cell epithelium are unknown. Nor is it known which Rap1 effectors mediate the direct control of adherens junction-actomyosin linkages in this context. The GTPase activating protein Rapgap1 acts as one regulatory layer controlling Rap1 α-Catenin modulation in regulating dorsal fold morphogenesis and is expressed in the ovary (Sawant et al., 2018; Wang et al., 2013). *Drosophila* has several known guanine nucleotide exchange factors (GEFs), including PDZ-GEF (also known as Dizzy), C3G, and Epac. Whether one or more GEFs have differential

functions during these stages of oogenesis, and in cell survival, remains to be tested. A well-known Rap1 effector, Cno, acts as a key signal relay mechanism downstream of Rap1. For example Cno mediates Rap1 functions in *Drosophila* morphogenesis including mesoderm invagination, head involution, and dorsal closure through modular biochemical functions (Perez-Vale et al., 2021; Sawyer et al., 2009). Whether these or other upstream and downstream regulators mediate Rap1 functions in epithelial tissue maintenance and cell survival remain to be determined.

Rap1 promotes follicle cell and polar cell survival during oogenesis

We found that Rap1 maintains epithelial cell viability during oogenesis. One possibility is that the role for Rap1 in adherens junction protein localization is coupled to cell survival. Cell-cell contacts are essential for cell viability in certain contexts (Guillot and Lecuit, 2013). We found that the adherens junction-cytoskeleton linker protein α-Catenin not only supported proper epithelial and tissue shapes, but also mildly promoted cell survival during oogenesis. Thus, cell-cell adhesions may be coupled to cell viability during tissue growth during oogenesis. Indeed, this period of dramatic tissue growth places extra strain on the epithelial follicle cells (Osswald et al., 2022), which could result in fewer cells surviving. Another major role for Rap1 was in promoting the survival of the mature polar cells, as well as other follicle cells. One possibility is that polar cell death could cause fewer border cells to be recruited to the cluster. Alternatively, or in addition, fewer polar cells and fewer border cells survive, thus resulting in a smaller border cell cluster. Having normal numbers of cells within the border cell cluster is critical for optimal migration speed and the ability to reach their final position at the oocyte (Cai et al., 2016; Stonko et al., 2015). Global downregulation of Rap1 also disrupted egg chamber health (here; Asha et al., 1999). Thus, Rap1's role in promoting cell viability is critical for normal oogenesis.

We do not yet have a clear understanding of the mechanism by which Rap1 promotes cell survival and suppresses apoptosis. Our results suggest that Rap1 may have independent functions in cell survival other than (or in addition to) regulation of adherens junction proteins. Although knocking down α-Catenin resulted in some apoptotic cells, this phenotype was overall much milder than that observed with Rap1 inhibition. Normally, DIAP1 must be maintained in the two mature polar cells to prevent their apoptosis (Borensztejn et al., 2013; Khammari et al., 2011). We observed a decrease in DIAP1 accumulation in the mature polar cells upon Rap1 inhibition, which is unlikely to be directly associated with defects in cell-cell adhesion. During stages 7 to 8, the overall levels of DIAP1 undergo a global reduction, which serves as a checkpoint mechanism to terminate unhealthy egg chambers rather than commit additional

nutritional and energy resources (Baum et al., 2007). Rap1 promotes levels of DIAP1, thus protecting the mature polar cells and likely other follicle cells from undergoing abnormal cell death. Moreover, expression of the p35 apoptosis inhibitor promoted survival of polar cells in Rap1-deficient border cell clusters, thus increasing the total number of migrating cells. It remains to be tested whether Rap1 generally maintains cell survival of follicle cells by more directly fine tuning DIAP1 levels at the molecular level, or if the regulation of DIAP1 by Rap1 is indirect, for example due to disruption of epithelial integrity when Rap1 is inhibited. It is also unclear how cellular mechanics function together with transcription of DIAP1 to promote cell survival during tissue growth of the ovary. Further work will also be needed to determine if the function for Rap1 in cell survival and maintenance of epithelial shapes in growing tissues is conserved in other developing tissues and organs.

MATERIALS AND METHODS

Drosophila genetics

All fly stocks used in this study are listed in Table 1 and the complete genotypes for each experiment can be found in Table 2. Crosses were typically set up and maintained at 25˚C. In cases where transgene expression impacted organism viability, the crosses were set up and maintained at 18˚C. The tub-GAL80ts ('tsGAL80') transgene (McGuire et al., 2004) was present in the genetic background of many crosses in this study to repress GAL4 expression during other stages of development. Flies were shifted to 29˚C for 12-72 hours prior to dissection to ensure optimal GAL4 expression and repression of tsGAL80, unless otherwise noted.

Immunostaining

Antibodies, sources, and dilutions used are listed in Table 3. Fly ovaries from 2- to 8-day old females were dissected in Schneider's *Drosophila* Medium (Thermo Fisher Scientific, Waltham, MA, USA) supplemented with 10% fetal bovine serum (Seradigm FBS; VWR, Radnor, PA, USA). Ovaries were either kept whole or dissected further into ovarioles (muscle sheath removed) and fixed for 10 mins using 16% methanol-free formaldehyde (Polysciences, Inc., Warrington, PA, USA) diluted to a final concentration of 4% in 1X Phosphate Buffered Saline (PBS). Following fixation, tissues were washed ≥4x with 'NP40 block' (50 mM Tris-HCL, pH 7.4, 150mM NaCl, 0.5% NP40, 5mg/ml bovine serum albumin [BSA]) and rocked in the solution for ≥30 mins prior to antibody incubation. Primary and secondary antibody incubation as well as all

other subsequent wash steps were also performed in NP40 block. Dissected and stained ovarioles and egg chambers were mounted on slides with Aqua-PolyMount (Polysciences, Inc.) media and allowed to harden prior to imaging.

Microscopy

Images of fixed egg chambers were acquired on a Zeiss LSM 880 confocal laser scanning microscope (KSU College of Veterinary Medicine Confocal Core) using either a 20 X 0.75 numerical aperture (NA) or a 40 X 1.3 NA oil-immersion objective controlled by Zeiss Zen 14 software.

Image Processing and Data Analysis

Measurements were performed using FIJI (Schindelin et al., 2012). Egg chambers were staged according to published criteria using morphological characteristics, such as the shape of the oocyte, presence of the yolk, or egg chamber aspect ratio (Chen et al., 2019; Spradling, 1993). Egg chamber local deformation measurements were determined by measuring the width between the apical follicle cell surfaces at 20% of the anterior-posterior (A-P) length of the egg chamber (the very anterior tip, opposite the oocyte, is considered to be 0% of the A-P length). In egg chambers with no obvious anterior point, or that had two anterior points, a medial point at the anterior end was used for measurement. Local deformation measurements were calculated for control egg chambers fixed both within the muscle sheath and with the muscle sheath removed prior to fixation. Tracings of the contact between the apical epithelial follicle cell surface and the germline nurse cells were performed to assess epithelial regularity and tissue packing (Fig. 2D,E). The line used to measure local deformation was used as a boundary. Tracings were then aligned by the flat edge, which represented the local deformation measurement, and scaled to enhance visibility. To further assess the tissue packing, cells were counted around the anterior perimeter using the local deformation measurement line as a boundary. To measure apical-basal cell heights, follicle cells were measured in single plane images of egg chambers that were dissected out of the muscle sheath. The line tool in Image J was used to measure the apical-basal cell heights for the three follicle cells found on either side of the polar cells. E-Cadherin staining was used to determine the limits of the apical and basal sides of each cell.

The polar cell aspect ratio was measured by analyzing Z-stacks taken of egg chambers stained with FasIII (to identify polar cells), E-Cadherin, and DAPI; the length and width was

measured at the widest point of each polar cell. The aspect ratio was then calculated by dividing the width by length.

E-Cadherin accumulation in polar cells (identified by FasIII) was measured by analyzing Z-stacks acquired of egg chambers stained for E-Cadherin, FasIII, and DAPI. A line was drawn to quantify pixel intensity starting at the apical polar cell-polar cell contact and extending to the basal polar cell surface (see line in Fig. 4A' and 4B'). Only images in which both polar cells could be viewed in the same Z-slice were used for quantitation. The "Plot Profile" function in FIJI was used to obtain a list of pixel intensity values that are plotted from apical to basal. These data were then arranged in a heat map with each lane representing a single polar cell pair with the top of each lane corresponding with the most apical intensity value and extending down to the most basal intensity value. Warmer tones represent higher pixel intensity. Staining and imaging conditions were kept consistent between samples. The signal distribution was analyzed by dividing the mean signal of the apical region of each line by the mean signal of a lateral segment.

Dying cells during oogenesis were quantified by scanning through dissected whole ovarioles stained and imaged for cDcp-1. Cells positive for caspase activity (cDcp-1-expressing cells) from stages 2 through 8 were quantified by stage; degenerating egg chambers were excluded from these analyses. Death of mature polar cells was scored by analyzing cDcp-1 expressing cells specifically in stage 7-8 egg chambers. DIAP1 accumulation in polar cells was assessed by acquiring Z-stacks of the anterior polar cells in stage 4-6 egg chambers prior to the global reduction of DIAP1 that occurs during stages 7-8. DIAP1 signals in polar cells were compared qualitatively to adjacent follicle cells. Polar cells were identified using a GFP protein trap in FasIII.

Quantification of the number of cells per border cell cluster was measured by acquiring Z-stacks through border cell clusters visualized using the nuclear envelope marker Lamin (also known as Lamin Dm_0) and DAPI. Whenever possible, E-Cadherin was used to determine the boundaries of fully delaminated border cell clusters. Z-stacks encompassing the entire cluster including both border cells and polar cells were acquired and nuclei were manually counted using the Lamin signal.

Border cell migration defects were scored at stage 10 of oogenesis. Border cell clusters were identified using E-Cadherin staining. The migration path was divided into four regions, beginning at the very anterior end (0%) and continuing to the oocyte (100%): 0-25%, 26-50%, 51-74%, and 75-100% completion. Any border cell clusters failing to reach 75% completion by stage 10 of oogenesis were considered to have failed to complete their migration.

Degenerating egg chambers were analyzed to assess the requirement of Rap1 in successful oogenesis. For each trial the same number of flies for experimental and control conditions were dissected. We then divide the number of degenerating egg chambers scored by the number of flies used for tissue to calculate the number of degenerating egg chambers per fly.

Reduction in polar cell number was scored using the cell fate marker Eya (expressed in all follicle cells except polar cells) and DAPI to label all nuclei. Extra polar cells were scored using the nuclear envelope marker Lamin and FasIII (labels polar cells at mid- to late-oogenesis).

Apical Myo-II accumulation was quantified by acquiring Z-stacks of stage 7-8 egg chambers expressing a fluorescent Myo-II reporter, Sqh::GFP, and co-stained for E-Cadherin and DAPI. A 2μm line was drawn at the apical surface of polar cells (identified by enrichment of E-Cadherin) and the "Plot Profile" function in FIJI was used to obtain a list of intensity values for each line. The intensity values were scaled to the highest pixel intensity measured in the experiment and plotted. Samples of inferior staining quality were eliminated from analysis. Staining and imaging conditions were kept consistent between samples.

Nuclear STAT intensity at stage 8 was quantified by measuring 10XSTAT::GFP reporter intensity by drawing lines across three nuclei on either side of polar cells The mean GFP intensity of each line was normalized to the mean DAPI signal for each nuclear measurement. All measurements were then normalized to the highest relative GFP intensity value measured in the experiment.

Figures, graphs, and statistics

Images were processed in FIJI and figures were assembled using Affinity Photo (Serif, Nottingham, United Kingdom). Illustrations were designed in Affinity Photo. Graphs and statistical tests were performed using GraphPad Prism 7 or Prism 9 (GraphPad Software, San Diego, CA, USA). All statistical tests and significance levels are listed in the figure legends for the figures in which they appear and in Table 4.

Acknowledgements

We would like to thank Denise Montell, Michelle Starz-Gaiano, Nick Brown, Sally Horne-Badovinac, and Hyung Don Ryoo, the Vienna *Drosophila* Resource Center (VDRC), the Bloomington *Drosophila* Stock Center (BDSC), and the Developmental Studies Hybridoma Bank (DSHB) at the University of Iowa for fly protocols, fly stocks, and antibodies. We also thank

Gibson Hoefgen and Manuel Garcia for general project assistance and maintenance of *Drosophila* strains and Emily Burghardt, Rehan Khan, and Yujun Chen for helpful comments on the manuscript. We acknowledge the Confocal Core, funded by the Kansas State University (KSU) College of Veterinary Medicine, which provided use of the Zeiss LSM 880 confocal microscope. We thank the KSU Statistics Consulting Laboratory for statistics advice. This work was supported by the National Science Foundation (NSF 2027617) to J.A.M. and a KSU Johnson Cancer Research Center Graduate Student Summer Stipend Award to C.L.M. and J.A.M. The authors declare no competing financial interests.

Author Contributions

C. Luke Messer: Conceptualization, Formal analysis, Validation, Investigation, Visualization, Methodology, Writing - Original Draft, Writing - Review & Editing; Jocelyn A. McDonald: Conceptualization, Supervision, Funding acquisition, Methodology, Writing - Original Draft, Writing - Review & Editing.

References

Abramson, J., Anderson, G., 2017. Thymic Epithelial Cells. Annual Review of Immunology 35, 85–118. https://doi.org/10.1146/annurev-immunol-051116-052320

Andersen, D., Horne-Badovinac, S., 2016. Influence of ovarian muscle contraction and oocyte growth on egg chamber elongation in Drosophila. Development 143, 1375–1387. https://doi.org/10.1242/dev.131276

Ando, K., Fukuhara, S., Moriya, T., Obara, Y., Nakahata, N., Mochizuki, N., 2013. Rap1 potentiates endothelial cell junctions by spatially controlling myosin II activity and actin organization. Journal of Cell Biology 202, 901–916. https://doi.org/10.1083/jcb.201301115

Asha, H., de Ruiter, N.D., Wang, M.G., Hariharan, I.K., 1999. The Rap1 GTPase functions as a regulator of morphogenesis invivo. The EMBO Journal 18, 605–615. https://doi.org/10.1093/emboj/18.3.605

Bach, E.A., Ekas, L.A., Ayala-Camargo, A., Flaherty, M.S., Lee, H., Perrimon, N., Baeg, G.-H., 2007. GFP reporters detect the activation of the Drosophila JAK/STAT pathway in vivo. Gene Expression Patterns 7, 323–331. https://doi.org/10.1016/j.modgep.2006.08.003

Balaji, R., Weichselberger, V., Classen, A.-K., 2019. Response of Drosophila epithelial cell and tissue shape to external forces in vivo. Development 146, dev171256. https://doi.org/10.1242/dev.171256

Baum, J.S., Arama, E., Steller, H., McCall, K., 2007. The Drosophila caspases Strica and Dronc function redundantly in programmed cell death during oogenesis. Cell Death and Differentiation 14, 1508–1517. https://doi.org/10.1038/sj.cdd.4402155

Beccari, S., Teixeira, L., Rørth, P., 2002. The JAK/STAT pathway is required for border cell migration during Drosophila oogenesis. Mechanisms of Development 111, 115–123. https://doi.org/10.1242/dev.120.8.2121

Blanpain, C., Fuchs, E., 2009. Epidermal homeostasis: a balancing act of stem cells in the skin. Nature reviews. Molecular cell biology 10, 207–17. https://doi.org/10.1038/nrm2636

Boettner, B., Harjes, P., Ishimaru, S., Heke, M., Fan, H.Q., Qin, Y., Van Aelst, L., Gaul, U., 2003. The AF-6 homolog canoe acts as a Rap1 effector during dorsal closure of the Drosophila embryo. Genetics 165, 159–69. https://doi.org/10.1093/genetics/165.1.159

Boettner, B., Van Aelst, L., 2007. The Rap GTPase Activator Drosophila PDZ-GEF Regulates Cell Shape in Epithelial Migration and Morphogenesis. Molecular and Cellular Biology 27, 7966–7980. https://doi.org/10.1128/MCB.01275-07

Bonello, T.T., Perez-Vale, K.Z., Sumigray, K.D., Peifer, M., 2018. Rap1 acts via multiple mechanisms to position Canoe and adherens junctions and mediate apical-basal polarity establishment. Development 145, dev157941. https://doi.org/10.1242/dev.157941

Borensztejn, A., Boissoneau, E., Fernandez, G., Agnès, F., Pret, A.M., 2013. JAK/STAT autocontrol of ligand-producing cell number through apoptosis. Development (Cambridge) 140, 195–204. https://doi.org/10.1242/dev.079046

Borensztejn, A., Mascaro, A., Wharton, K.A., 2018. JAK/STAT signaling prevents excessive apoptosis to ensure maintenance of the interfollicular stalk critical for Drosophila oogenesis. Developmental Biology 438, 1–9. https://doi.org/10.1016/j.ydbio.2018.03.018

Bröer, S., 2008. Amino acid transport across mammalian intestinal and renal epithelia. Physiological reviews 88, 249–86. https://doi.org/10.1152/physrev.00018.2006

Cai, D., Dai, W., Prasad, M., Luo, J., Gov, N.S., Montell, D.J., 2016. Modeling and analysis of collective cell migration in an in vivo three-dimensional environment. Proceedings of the National Academy of Sciences of the United States of America 113, E2134–E2141. https://doi.org/10.1073/pnas.1522656113

Chang, Y.-C., Wu, J.-W., Hsieh, Y.-C., Huang, T.-H., Liao, Z.-M., Huang, Y.-S., Mondo, J.A., Montell, D., Jang, A.C.-C., 2018. Rap1 Negatively Regulates the Hippo Pathway to

Polarize Directional Protrusions in Collective Cell Migration. Cell Reports 22, 2160–2175. https://doi.org/10.1016/j.celrep.2018.01.080
Chen, D.-Y., Crest, J., Streichan, S.J., Bilder, D., 2019. Extracellular matrix stiffness cues junctional remodeling for 3D tissue elongation. Nat Commun 10, 3339. https://doi.org/10.1038/s41467-019-10874-x
Choi, W., Harris, N.J., Sumigray, K.D., Peifer, M., 2013. Rap1 and Canoe/afadin are essential for establishment of apical-basal polarity in the Drosophila embryo. Molecular biology of the cell 24, 945–63. https://doi.org/10.1091/mbc.E12-10-0736
Clem, R.J., Fechheimer, M., Miller, L.K., 1991. Prevention of Apoptosis by a Baculovirus Gene During Infection of Insect Cells. Science 254, 1388–1390. https://doi.org/10.1126/science.1962198
Crest, J., Diz-Muñoz, A., Chen, D.-Y., Fletcher, D.A., Bilder, D., 2017. Organ sculpting by patterned extracellular matrix stiffness. eLife 6, e24958. https://doi.org/10.7554/eLife.24958
Duhart, J.C., Parsons, T.T., Raftery, L.A., 2017. The repertoire of epithelial morphogenesis on display: Progressive elaboration of Drosophila egg structure. Mechanisms of Development 148, 18–39. https://doi.org/10.1016/j.mod.2017.04.002
Duszyc, K., Gomez, G.A., Schroder, K., Sweet, M.J., Yap, A.S., 2017. In life there is death: How epithelial tissue barriers are preserved despite the challenge of apoptosis. Tissue Barriers 5, e1345353–e1345353. https://doi.org/10.1080/21688370.2017.1345353
Gloerich, M., Bos, J.L., 2011. Regulating Rap small G-proteins in time and space. Trends in Cell Biology 21, 615–623. https://doi.org/10.1016/j.tcb.2011.07.001
Grammont, M., Irvine, K.D., 2002. Organizer activity of the polar cells during Drosophila oogenesis. Development 129, 5131–5140. https://doi.org/10.1242/dev.129.22.5131
Guillot, C., Lecuit, T., 2013. Mechanics of epithelial tissue homeostasis and morphogenesis. Science (New York, N.Y.) 340, 1185–9. https://doi.org/10.1126/science.1235249
Haigo, S.L., Bilder, D., 2011. Global Tissue Revolutions in a Morphogenetic Movement Controlling Elongation. Science 331, 1071–1074. https://doi.org/10.1126/science.1199424
Haigo, S.L., Hildebrand, J.D., Harland, R.M., Wallingford, J.B., 2003. Shroom induces apical constriction and is required for hingepoint formation during neural tube closure. Curr Biol 13, 2125–2137. https://doi.org/10.1016/j.cub.2003.11.054
Harris, T.J.C., Tepass, U., 2010. Adherens junctions: from molecules to morphogenesis. Nat Rev Mol Cell Biol 11, 502–514. https://doi.org/10.1038/nrm2927
Hay, B.A., Wassarman, D.A., Rubin, G.M., 1995. Drosophila homologs of baculovirus inhibitor of apoptosis proteins function to block cell death. Cell 83, 1253–1262. https://doi.org/10.1016/0092-8674(95)90150-7
Hay, B.A., Wolff, T., Rubin, G.M., 1994. Expression of baculovirus P35 prevents cell death in Drosophila. Development 120, 2121–2129. https://doi.org/10.1242/dev.120.8.2121
Hayashi, S., Ito, K., Sado, Y., Taniguchi, M., Akimoto, A., Takeuchi, H., Aigaki, T., Matsuzaki, F., Nakagoshi, H., Tanimura, T., Ueda, R., Uemura, T., Yoshihara, M., Goto, S., 2002. GETDB, a database compiling expression patterns and molecular locations of a collection of Gal4 enhancer traps. Genesis 34, 58–61. https://doi.org/10.1002/gene.10137
Hudson, A.M., Petrella, L.N., Tanaka, A.J., Cooley, L., 2008. Mononuclear muscle cells in Drosophila ovaries revealed by GFP protein traps. Dev Biol 314, 329–340. https://doi.org/10.1016/j.ydbio.2007.11.029
Irvine, K.D., Wieschaus, E., 1994. Cell intercalation during Drosophila germband extension and its regulation by pair-rule segmentation genes. Development 120, 827–841. https://doi.org/10.1242/dev.120.4.827

Keller, R.E., 1981. An experimental analysis of the role of bottle cells and the deep marginal zone in gastrulation ofXenopus laevis. Journal of Experimental Zoology 216, 81–101. https://doi.org/10.1002/jez.1402160109
Khammari, A., Agnès, F., Gandille, P., Pret, A.-M., 2011. Physiological apoptosis of polar cells during Drosophila oogenesis is mediated by Hid-dependent regulation of Diap1. Cell Death & Differentiation 18, 793–805. https://doi.org/10.1038/cdd.2010.141
Kim, Y.S., Fan, R., Lith, S.C., Dicke, A.-K., Drexler, H.C.A., Kremer, L., Kuempel-Rink, N., Hekking, L., Stehling, M., Bedzhov, I., 2022. Rap1 controls epiblast morphogenesis in sync with the pluripotency states transition. Dev Cell 57, 1937-1956.e8. https://doi.org/10.1016/j.devcel.2022.07.011
Knox, A.L., Brown, N.H., 2002. Rap1 GTPase Regulation of Adherens Junction Positioning and Cell Adhesion. Science 295, 1285–1288. https://doi.org/10.1126/science.1067549
Lebo, D.P.V., McCall, K., 2021. Murder on the Ovarian Express: A Tale of Non-Autonomous Cell Death in the Drosophila Ovary. Cells 10, 1454. https://doi.org/10.3390/cells10061454
Li, M., Sun, S., Priest, J., Bi, X., Fan, Y., 2019. Characterization of TNF-induced cell death in Drosophila reveals caspase- and JNK-dependent necrosis and its role in tumor suppression. Cell Death & Disease 10, 613–613. https://doi.org/10.1038/s41419-019-1862-0
Loyer, N., Kolotuev, I., Pinot, M., Le Borgne, R., 2015. Drosophila E-cadherin is required for the maintenance of ring canals anchoring to mechanically withstand tissue growth. Proceedings of the National Academy of Sciences 112, 12717–12722. https://doi.org/10.1073/pnas.1504455112
Martin, A.C., Goldstein, B., 2014. Apical constriction: themes and variations on a cellular mechanism driving morphogenesis. Development 141, 1987–1998. https://doi.org/10.1242/dev.102228
Martin, A.C., Kaschube, M., Wieschaus, E.F., 2009. Pulsed contractions of an actin-myosin network drive apical constriction. Nature 457, 495–9. https://doi.org/10.1038/nature07522
McGuire, S.E., Mao, Z., Davis, R.L., 2004. Spatiotemporal gene expression targeting with the TARGET and gene-switch systems in Drosophila. Sci STKE 2004, pl6. https://doi.org/10.1126/stke.2202004pl6
Munjal, A., Lecuit, T., 2014. Actomyosin networks and tissue morphogenesis. Development 141, 1789–1793. https://doi.org/10.1242/dev.091645
Niewiadomska, P., Godt, D., Tepass, U., 1999. DE-Cadherin Is Required for Intercellular Motility during Drosophila Oogenesis. Journal of Cell Biology 144, 533–547. https://doi.org/10.1083/jcb.144.3.533
Osswald, M., Barros-Carvalho, A., Carmo, A.M., Loyer, N., Gracio, P.C., Sunkel, C.E., Homem, C.C.F., Januschke, J., Morais-de-Sá, E., 2022. aPKC regulates apical constriction to prevent tissue rupture in the Drosophila follicular epithelium. Curr Biol 32, 4411-4427.e8. https://doi.org/10.1016/j.cub.2022.08.063
Peifer, M., Orsulic, S., Sweeton, D., Wieschaus, E., 1993. A role for the Drosophila segment polarity gene armadillo in cell adhesion and cytoskeletal integrity during oogenesis. Development 118, 1191–1207. https://doi.org/10.1242/dev.118.4.1191
Perez-Vale, K.Z., Yow, K.D., Gurley, N.J., Greene, M., Peifer, M., 2022. Rap1 regulates apical contractility to allow embryonic morphogenesis without tissue disruption and acts in part via Canoe-independent mechanisms. Mol Biol Cell mbcE22050176. https://doi.org/10.1091/mbc.E22-05-0176
Perez-Vale, K.Z., Yow, K.D., Johnson, R.I., Byrnes, A.E., Finegan, T.M., Slep, K.C., Peifer, M., 2021. Multivalent interactions make adherens junction–cytoskeletal linkage robust during

morphogenesis. Journal of Cell Biology 220, e202104087. https://doi.org/10.1083/jcb.202104087
Potla, U., Ni, J., Vadaparampil, J., Yang, G., Leventhal, J.S., Campbell, K.N., Chuang, P.Y., Morozov, A., He, J.C., D'Agati, V.D., Klotman, P.E., Kaufman, L., 2014. Podocyte-specific RAP1GAP expression contributes to focal segmental glomerulosclerosis-associated glomerular injury. The Journal of clinical investigation 124, 1757–69. https://doi.org/10.1172/JCI67846
Royou, A., Field, C., Sisson, J.C., Sullivan, W., Karess, R., 2004. Reassessing the Role and Dynamics of Nonmuscle Myosin II during Furrow Formation in Early Drosophila Embryos. Molecular Biology of the Cell 15, 838–850. https://doi.org/10.1091/mbc.e03-06-0440
Ruohola, H., Bremer, K.A., Baker, D., Swedlow, J.R., Jan, L.Y., Jan, Y.N., 1991. Role of neurogenic genes in establishment of follicle cell fate and oocyte polarity during oogenesis in Drosophila. Cell 66, 433–449. https://doi.org/10.1016/0092-8674(81)90008-8
Sarpal, R., Pellikka, M., Patel, R.R., Hui, F.Y.W., Godt, D., Tepass, U., 2012. Mutational analysis supports a core role for Drosophila α-Catenin in adherens junction function. Journal of Cell Science 125, 233–245. https://doi.org/10.1242/jcs.096644
Sasaki, K., Kojitani, N., Hirose, H., Yoshihama, Y., Suzuki, H., Shimada, M., Takayanagi, A., Yamashita, A., Nakaya, M., Hirano, H., Takahashi, H., Ohno, S., 2020. Shank2 Binds to aPKC and Controls Tight Junction Formation with Rap1 Signaling during Establishment of Epithelial Cell Polarity. Cell Reports 31, 107407. https://doi.org/10.1016/j.celrep.2020.02.088
Sawant, K., Chen, Y., Kotian, N., Preuss, K.M., McDonald, J.A., 2018. Rap1 GTPase promotes coordinated collective cell migration in vivo. Molecular Biology of the Cell 29, 2656–2673. https://doi.org/10.1091/mbc.E17-12-0752
Sawyer, J.K., Harris, N.J., Slep, K.C., Gaul, U., Peifer, M., 2009. The Drosophila afadin homologue Canoe regulates linkage of the actin cytoskeleton to adherens junctions during apical constriction. Journal of Cell Biology 186, 57–73. https://doi.org/10.1083/jcb.200904001
Schindelin, J., Arganda-Carreras, I., Frise, E., Kaynig, V., Longair, M., Pietzsch, T., Preibisch, S., Rueden, C., Saalfeld, S., Schmid, B., Tinevez, J.-Y., White, D.J., Hartenstein, V., Eliceiri, K., Tomancak, P., Cardona, A., 2012. Fiji: an open-source platform for biological-image analysis. Nat Methods 9, 676–682. https://doi.org/10.1038/nmeth.2019
Schoborg, T.A., Smith, S.L., Smith, L.N., Morris, H.D., Rusan, N.M., 2019. Micro-computed tomography as a platform for exploring Drosophila development. Development 146, dev176685. https://doi.org/10.1242/dev.176685
Silver, D.L., Montell, D.J., 2001. Paracrine Signaling through the JAK/STAT Pathway Activates Invasive Behavior of Ovarian Epithelial Cells in Drosophila. Cell 107, 831–841. https://doi.org/10.1016/S0092-8674(01)00607-9
Smutny, M., Cox, H.L., Leerberg, J.M., Kovacs, E.M., Conti, M.A., Ferguson, C., Hamilton, N.A., Parton, R.G., Adelstein, R.S., Yap, A.S., 2010. Myosin II isoforms identify distinct functional modules that support integrity of the epithelial zonula adherens. Nat Cell Biol 12, 696–702. https://doi.org/10.1038/ncb2072
Spahn, P., Ott, A., Reuter, R., 2012. The PDZ-GEF protein Dizzy regulates the establishment of adherens junctions required for ventral furrow formation in Drosophila. J Cell Sci 125, 3801–3812. https://doi.org/10.1242/jcs.101196
Spradling, A.C., 1993. Developmental genetics of oogenesis., in: The Development of Drosophila Melanogaster. Cold Spring Harbor Laboratory Press, Cold Spring Harbor, NY, pp. 1–70.

Starz-Gaiano, M., Melani, M., Wang, X., Meinhardt, H., Montell, D.J., 2008. Feedback Inhibition of JAK/STAT Signaling by Apontic Is Required to Limit an Invasive Cell Population. Developmental Cell 14, 726–738. https://doi.org/10.1016/j.devcel.2008.03.005

Stonko, D.P., Manning, L., Starz-Gaiano, M., Peercy, B.E., 2015. A mathematical model of collective cell migration in a three-dimensional, heterogeneous environment. PloS one 10, e0122799–e0122799. https://doi.org/10.1371/journal.pone.0122799

Tai, K., Cockburn, K., Greco, V., 2019. Flexibility sustains epithelial tissue homeostasis. Current opinion in cell biology 60, 84–91. https://doi.org/10.1016/j.ceb.2019.04.009

Tanentzapf, G., Smith, C., McGlade, J., Tepass, U., 2000. Apical, lateral, and basal polarization cues contribute to the development of the follicular epithelium during Drosophila oogenesis. J Cell Biol 151, 891–904. https://doi.org/10.1083/jcb.151.4.891

Valer, F.B., Machado, M.C.R., Silva-Junior, R.M.P., Ramos, R.G.P., 2018. Expression of Hbs, Kirre, and Rst during Drosophila ovarian development. Genesis 56, e23242. https://doi.org/10.1002/dvg.23242

Vasudevan, D., Ryoo, H.D., 2016. Detection of Cell Death in Drosophila Tissues. Methods Mol Biol 1419, 131–144. https://doi.org/10.1007/978-1-4939-3581-9_11

Wang, A., Dunn, A.R., Weis, W.I., 2022. Mechanism of the cadherin–catenin F-actin catch bond interaction. eLife 11, e80130. https://doi.org/10.7554/eLife.80130

Wang, Y.-C., Khan, Z., Wieschaus, E.F., 2013. Distinct Rap1 activity states control the extent of epithelial invagination via α-catenin. Developmental cell 25, 299–309. https://doi.org/10.1016/j.devcel.2013.04.002

Williams-Masson, E.M., Malik, A.N., Hardin, J., 1997. An actin-mediated two-step mechanism is required for ventral enclosure of the C. elegans hypodermis. Development 124, 2889–2901. https://doi.org/10.1242/dev.124.15.2889

Yan, N., Wu, J.-W., Chai, J., Li, W., Shi, Y., 2004. Molecular mechanisms of DrICE inhibition by DIAP1 and removal of inhibition by Reaper, Hid and Grim. Nature structural & molecular biology 11, 420–8. https://doi.org/10.1038/nsmb764

Yonemura, S., Wada, Y., Watanabe, T., Nagafuchi, A., Shibata, M., 2010. α-Catenin as a tension transducer that induces adherens junction development. Nat Cell Biol 12, 533–542. https://doi.org/10.1038/ncb2055

Figures and Figure Legends

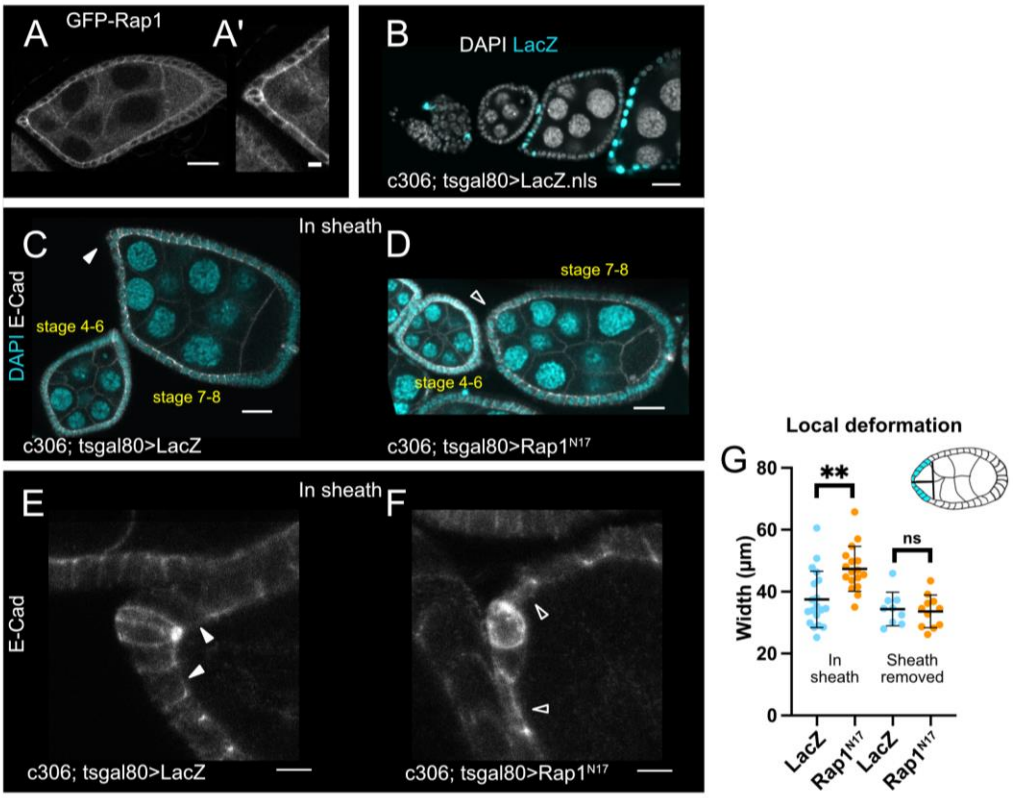

Figure 1. Rap1 is required in the anterior epithelium to maintain follicle cell and egg chamber shapes

(A-A') Egg chamber with GFP tagged Rap1 illustrates Rap1 enrichment in follicle cells. (A') Close-up of anterior epithelium from the same egg chamber showing apical Rap1 accumulation in anterior epithelium and polar cells. (B) Ovariole expressing UAS-LacZ driven by *c306*-GAL4 to demonstrate the *c306*-GAL4 expression pattern. (C-D) LacZ control (C) or DN-Rap1^{N17} (D) egg chambers fixed in the muscle sheath. Anterior epithelia are distorted at stages 7-8 in DN-Rap1^{N17}. Arrowheads indicate anterior region of stage 7-8 egg chambers. Solid arrowhead points to normal anterior epithelium of control (C), while open arrowhead indicates distorted anterior region for DN-Rap1^{N17} (D). (E, F) Close-up views of anterior regions of stage 7-8 egg chambers showing normal anterior epithelium in control (E, solid arrowheads) and distorted epithelium in DN-Rap1^{N17} (F, open arrowheads). (G) Quantification of local deformation measures taken at 20% of egg chamber length (illustrated by egg chamber schematic) for egg chambers fixed in sheath and fixed after the sheath was removed. ** p≤0.01 two-tailed unpaired t-test. N≥9 egg chambers measured per genotype for each condition. (A-D) Scale bars 20µm. (A', E, F) Scale bars 5µm. Anterior is to the left in this and the following figures.

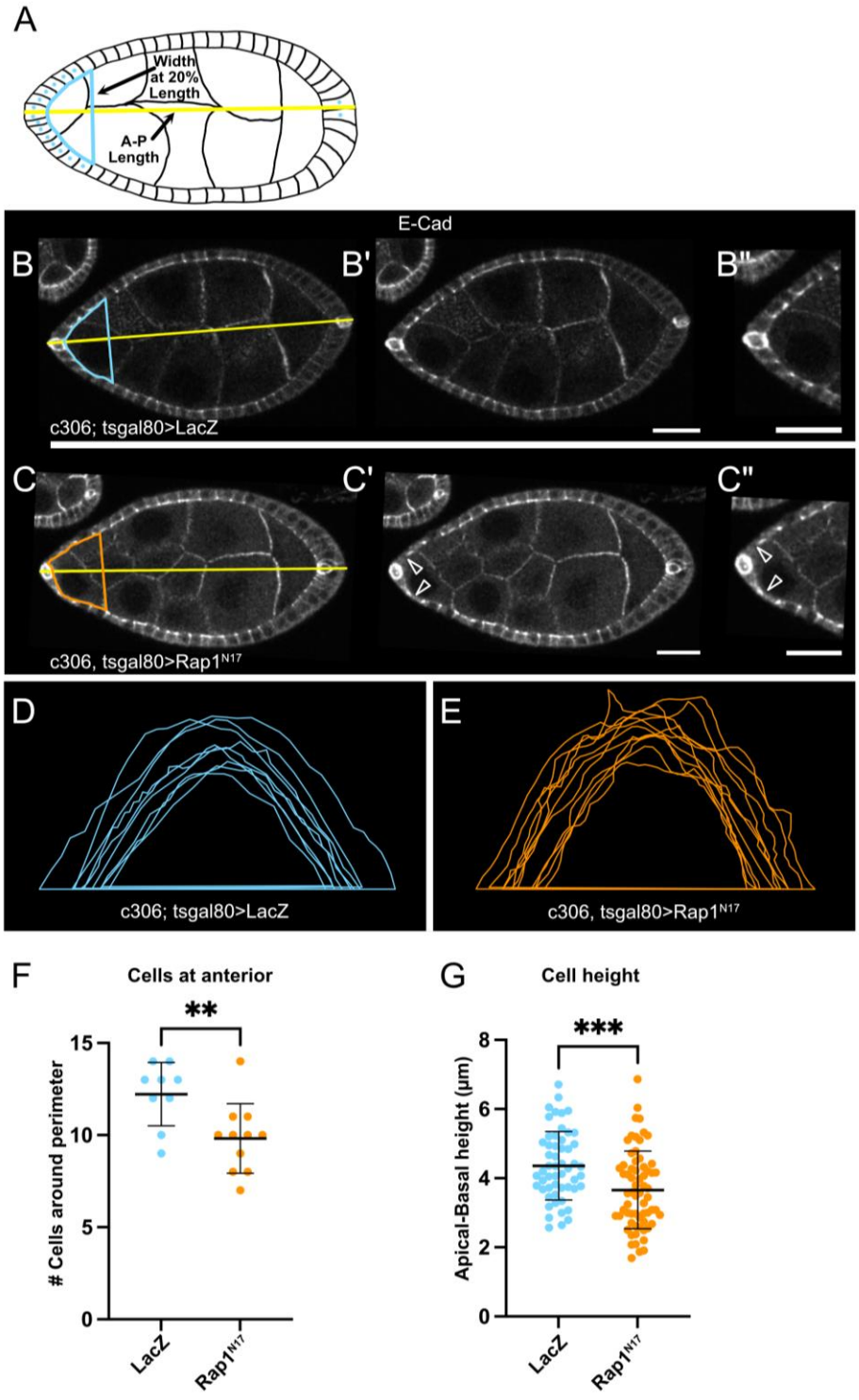

Figure 2. The cell shape maintenance function of Rap1 is independent of tissue packing

(A) Schematic of local deformation measurement and anterior tracings used to assess epithelial shapes. (B-C") Egg chambers dissected out of muscle sheath before fixation for LacZ (B) and

DN-Rap1^{N17} (C). Yellow lines (B, C) indicate egg chamber length along anterior-posterior axis. Outlined regions in blue (B) or orange (C) indicate the region of anterior tracings used to assess epithelial regularity in the anterior (20%) of egg chambers. (B', C') Same as B-C with overlays removed for clarity. (B", C") Close-up views of anterior epithelia from the same egg chambers in (B and C). Arrowheads indicate local epithelial defects observed in DN-Rap1^{N17}. (D-E) Tracings of anterior apical cell surfaces for LacZ (D) and DN-Rap1^{N17} (E). Tracings in E are more variable and lack the uniformity of those in D. (F) Quantification of cells around the anterior perimeter for control and DN-Rap1^{N17} egg chambers dissected out of the muscle sheath before fixation. DN-Rap1^{N17} egg chambers have fewer cells per area suggesting that the follicle cells are more spaced out or stretched. ** $p \leq 0.01$ two-tailed unpaired t test. $N \geq 9$ egg chambers per genotype. (G) Quantification of apical-basal cell heights for the three follicle cells on either side of the anterior polar cell pair. *** $p \leq 0.001$ two-tailed unpaired t test. $N \geq 54$ cells per genotype. Scale bars 20μm.

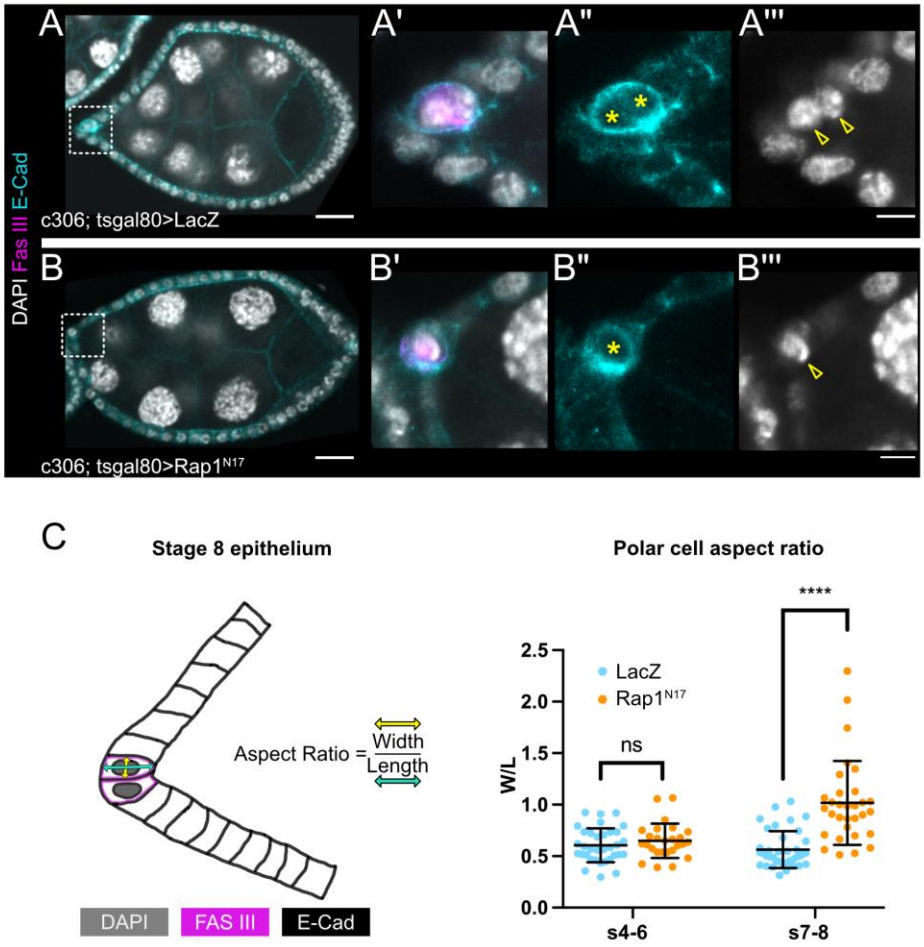

Figure 3. Rap1 is required for proper polar cell shape

(A-B) Examples of LacZ (A) and DN-Rap1^{N17} (B) stage 7 egg chambers imaged for polar cell shape. Dashed boxes indicate the regions of close-up views of the anterior regions shown in (A'-A''', B'-B'''). Asterisks (A", B") or arrowheads (A''', B''') indicate polar cells in single channel images. (B'-B''') Only one spherical polar cell is present. (C) Aspect ratio schematic and quantification. Aspect ratio (AR) was defined as the dorsoventral (DV, yellow arrow) width divided by the anterior-posterior (AP, cyan arrow) length. AR measurements plotted for stage 4-6 and stage 7-8 egg chamber polar cells. DN-Rap1^{N17} polar cells are more spherical at stage 7-8 indicated by average AR=1.02 vs average AR=0.56 for control. **** $p<0.0001$ two-tailed unpaired t test. N≥26 polar cells measured per genotype per egg chamber stage. (A, B) Scale bars 20μm. (A''', B''') Scale bars 5μm.

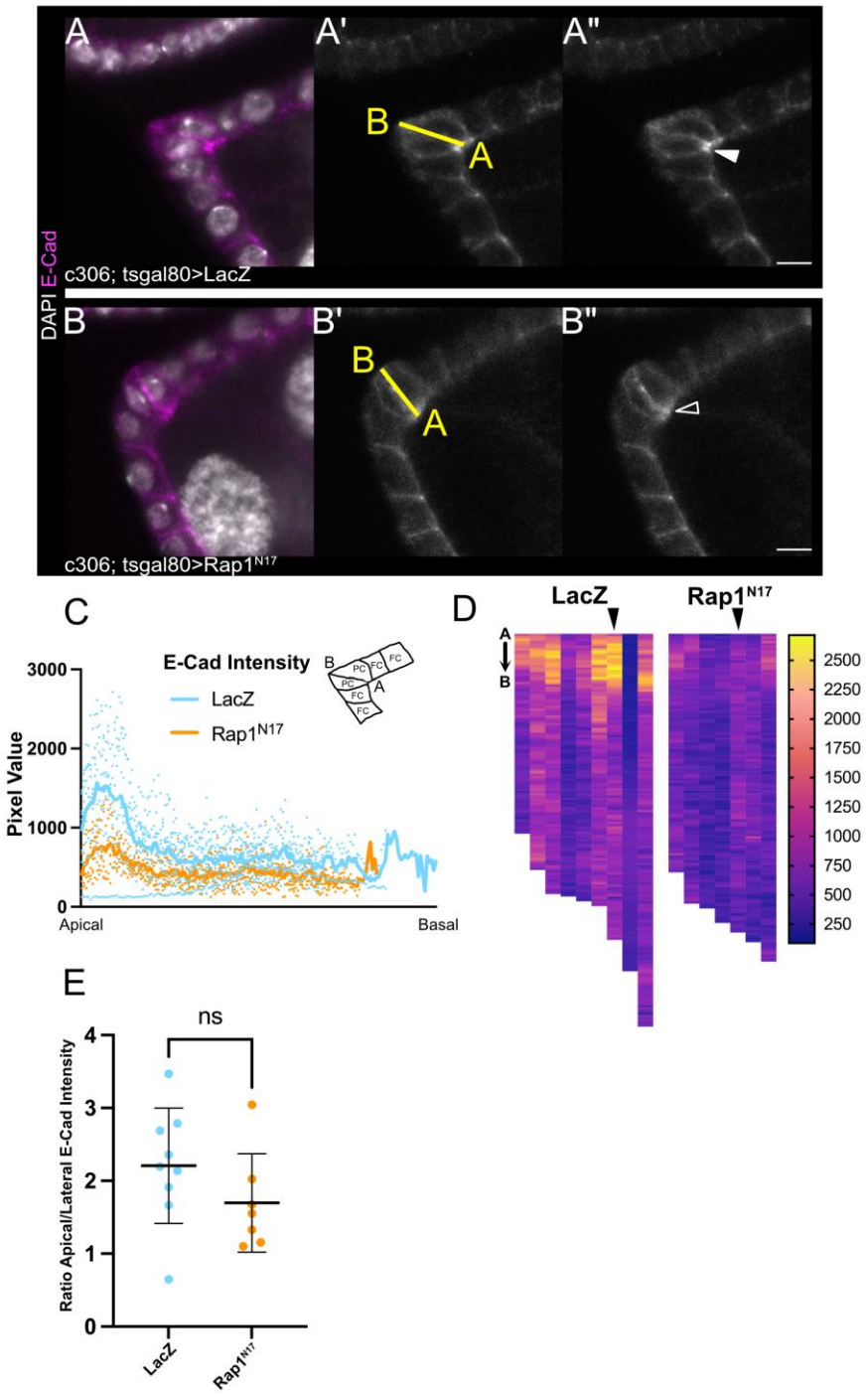

Figure 4. Rap1 is required for apical E-Cadherin enrichment in polar cells

(A-B) Anterior regions of stage 7-8 egg chambers for LacZ control (A) and DN-Rap1^{N17} egg chambers (B). (A'-B") Single channel panels from A and B showing E-Cadherin (gray) enrichment. (A', B') Yellow line indicates region of measurement beginning at the apical polar cell-polar cell contact ("*A*") and ending at the basal polar cell-polar cell interface ("*B*"). (A", B") Same as A' and B' without line overlays for clarity. Solid arrowhead indicates apical

accumulation of E-Cadherin in A”. Open arrowhead indicates reduced E-Cadherin enrichment in B”. Image brightness adjusted for presentation purposes. (C) Measurement schematic and quantification of fluorescence intensities measured along lines drawn as in A’ and B’. Lines represent mean intensity. (D) Heat map representation of pixel intensity values plotted in C. Arrowheads at the top of heat map indicate the lanes corresponding to the images shown in A” and B”. Each lane is one polar cell pair with anterior intensity values starting at the top and extending to basal intensity values at the bottom. (E) Quantification of apicolateral ratio of E-Cadherin intensity. ns two-tailed unpaired t test. N≥7 egg chambers per genotype. Scale bars 5μm.

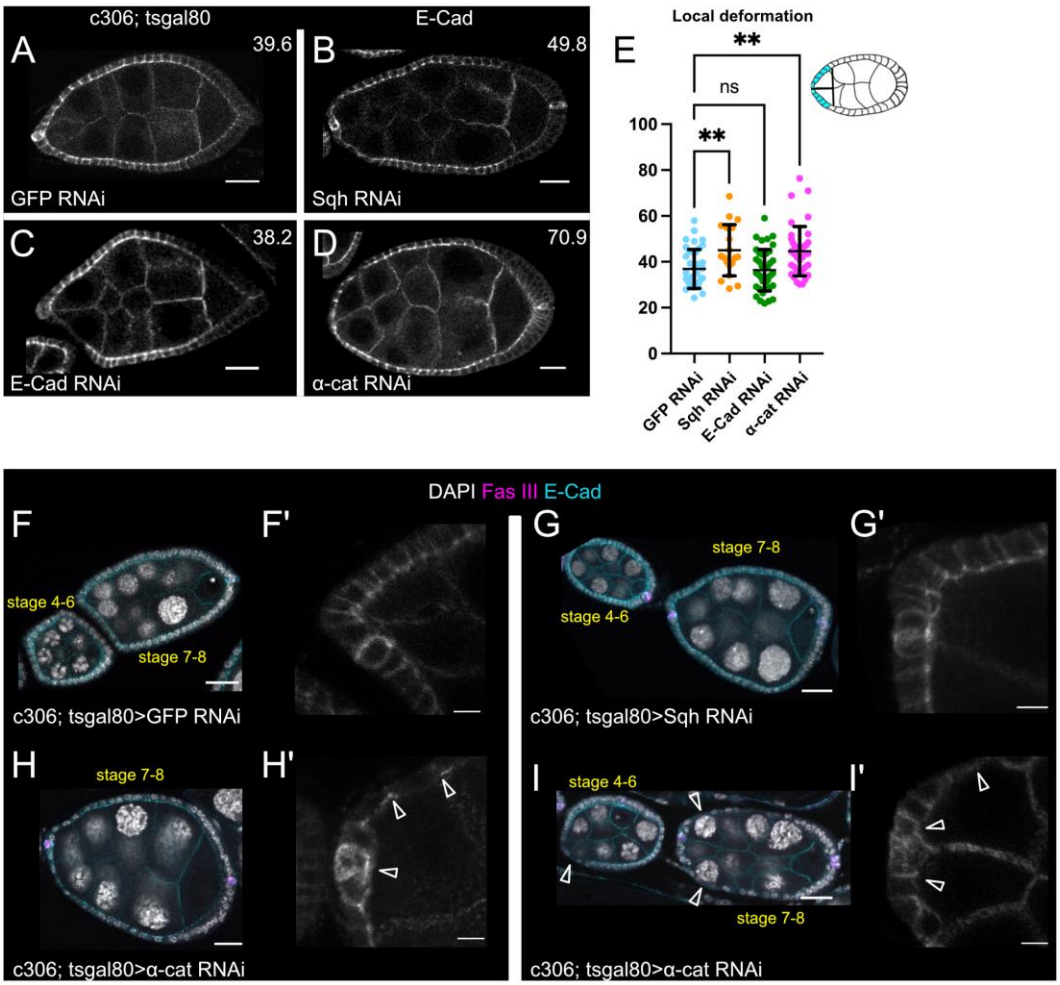

Figure 5. Sqh and α-Catenin maintain local tissue shape and α-Catenin is required for epithelial integrity

(A-D) Examples of stage 8 GFP RNAi (A), Sqh RNAi (B), E-Cadherin RNAi (C), and α-cat RNAi (D) egg chambers imaged for egg chamber shape. Numbers at top right of each panel correspond to the local deformation measurement acquired for each egg chamber. (E) Schematic and quantification of local deformation measurement. ** p≤0.01 One-way ANOVA followed by Dunnett's multiple comparisons test. N≥19 egg chambers per genotype. (F-I) Examples of GFP RNAi (F), Sqh RNAi (G), and α-cat RNAi (H-I) ovarioles imaged to show egg chamber shape and anterior epithelium. (F'-I') Maximum intensity projections of close-up views of the E-Cadherin channel (gray) at anterior regions of stage 7-8 egg chambers pictured in the main panels. Open arrowheads in H', I, and I' indicate "stretched" or "irregularly shaped" cells observed in α-cat RNAi egg chambers. (A-D, F-I) Scale bars 20μm. (F'-I') Scale bars 5μm.

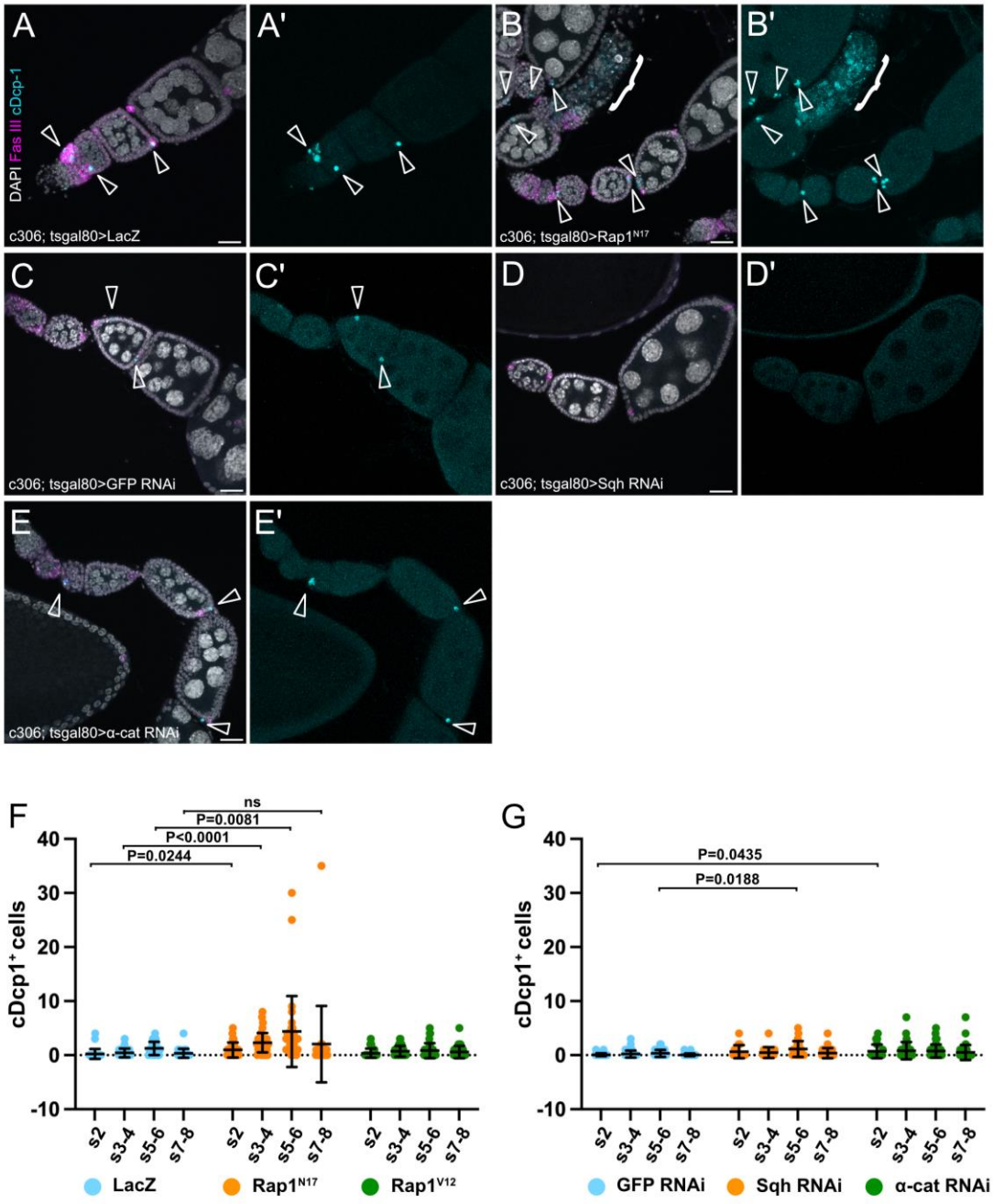

Figure 6. Rap1 and α-Catenin are required for cell viability during oogenesis

(A-E) Maximum intensity projections of ovarioles showing caspase positive cells for LacZ (A), DN-Rap1^{N17} (B), GFP RNAi (C), Sqh RNAi (D), and α-cat RNAi (E). (A'-E') Single channel images show cDcp1 accumulation. Open arrowheads indicate cDcp1 positive cells and the bracket in B-B' indicates a degenerating egg chamber. (F-G) Quantification of cDcp1 positive

cells for the indicated egg chamber stages. One-way ANOVA followed by Dunnett's multiple comparisons test. N≥14 egg chambers per stage per genotype. Scale bars 20μm.

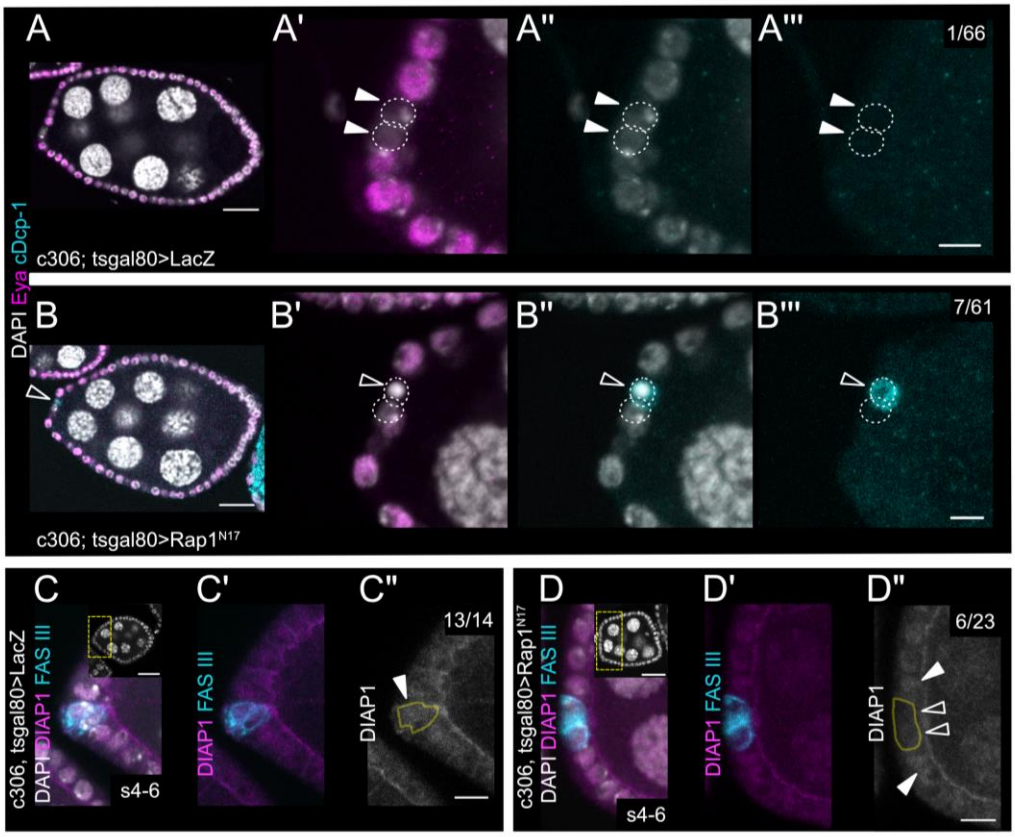

Figure 7. Rap1 is required for polar cell viability and proper DIAP1 accumulation

(A-B) Stage 7-8 LacZ (A) and DN-Rap1^{N17} (B) egg chambers scored for cDcp1 positive polar cells. (A'-B''') Close-up views of the anterior region of egg chambers pictured in A and B. Filled arrowheads in A'-A''' indicate viable mature polar cells. Open arrowheads in B'-B''' indicate a cDcp1 positive dying polar cell. Numbers in A''' and B''' indicate the number of egg chambers with cDcp1 positive polar cells out of total stage 7-8 egg chambers scored. Dashed circles outline polar cells in A'-B'''. (C-D") Stage 4-6 LacZ (C-C") and DN-Rap1^{N17} (D-D") egg chambers imaged for DIAP1 accumulation in polar cells. (C, D) Insets show DAPI-stained whole egg chambers corresponding to close-up regions, with yellow boxes outlining the approximate region depicted in main panels. (C', D') DIAP1 and FasIII:GFP. (C", D") DIAP1 alone; the polar cells are outlined in yellow based on the FasIII:GFP signal in (C', D'). Solid arrowheads indicate normal DIAP1 accumulation. Open arrowheads indicate reduced DIAP1. The number of polar cell pairs with normal DIAP1 accumulation out of total egg chambers scored is reported in the upper right of C", D". (A, B) Scale bars 20μm. (C, D) Inset scale bars 20μm. (A''', B''', C", D") Scale bars 5μm.

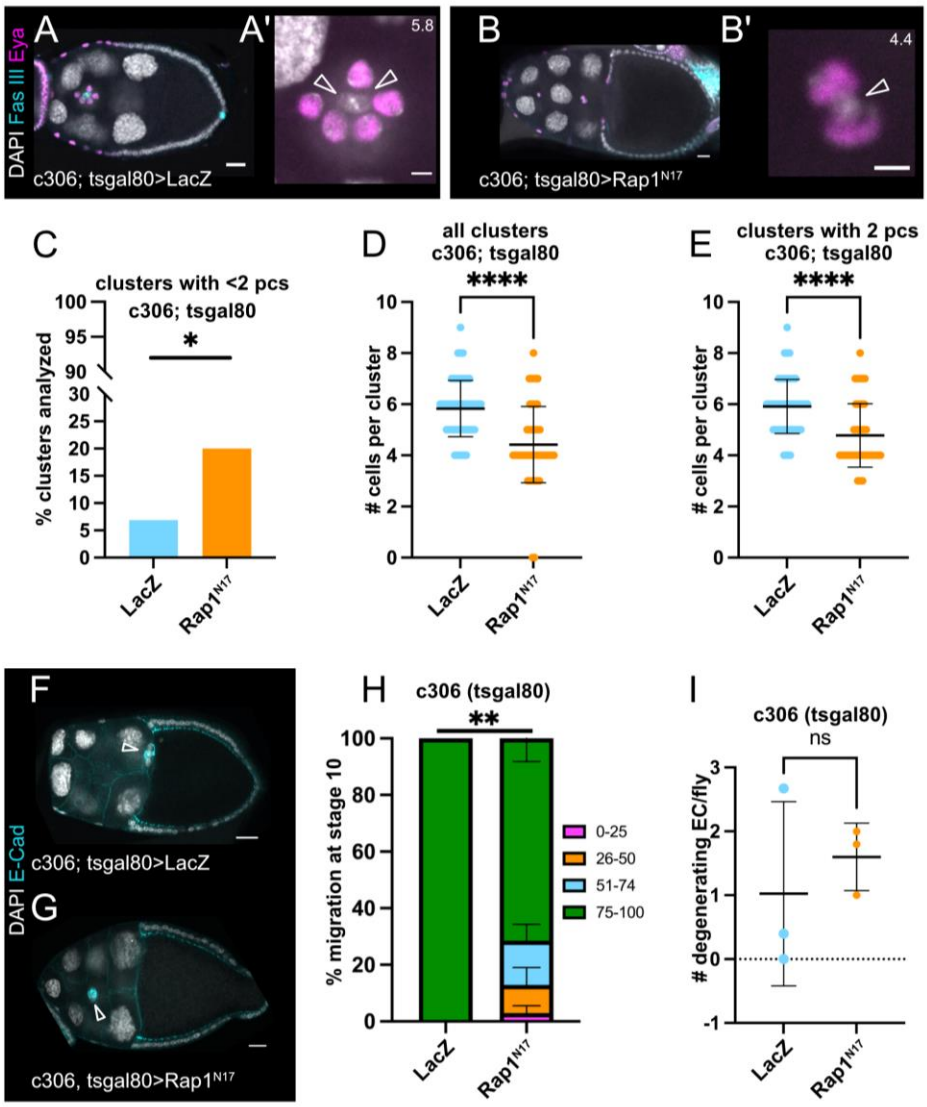

Figure 8. Rap1 is required for proper border cell cluster assembly and migration

(A-B) Stages 9-10 LacZ (A) and DN-Rap1^{N17} (B) egg chambers. (A'-B') Close-up views of border cell clusters from egg chambers pictured in A and B showing only Eya (magenta) and DAPI (gray). Arrowheads indicate polar cells. The numbers at top right are the average number of cells observed in border cell clusters for each genotype. (C) Quantification of border cell clusters with <2 polar cells for each genotype. * $p<0.05$ two-sided Fisher's exact test. N≥85 border cell clusters per genotype. (D) Quantification of total cell number per cluster for all clusters analyzed. **** $p<0.0001$ two-tailed unpaired t test. N≥85 border cell clusters per genotype. (E) Quantification of total cell number per cluster for clusters with 2 pcs. **** $p<0.0001$ two-tailed unpaired t test. N≥68 border cell clusters per genotype. (F-G) Stage 10 LacZ (F) and DN-Rap1^{N17} (G) egg chambers showing the location of border cells. DN-Rap1^{N17}

border cells do not complete their migration (G); in this example, the border cells migrated ~40% of the normal migration distance. Arrowheads indicate the border cell clusters. (H) Quantification of migration defects for each genotype. ** p≤0.01 two-tailed unpaired t test. N≥57 egg chambers per genotype. (I) Quantification of degenerating egg chambers observed per fly for each genotype. ns two-tailed unpaired t test. N=10 flies per genotype. (A, B, F, G) Scale bars 20μm. (A', B') Scale bars 5μm.

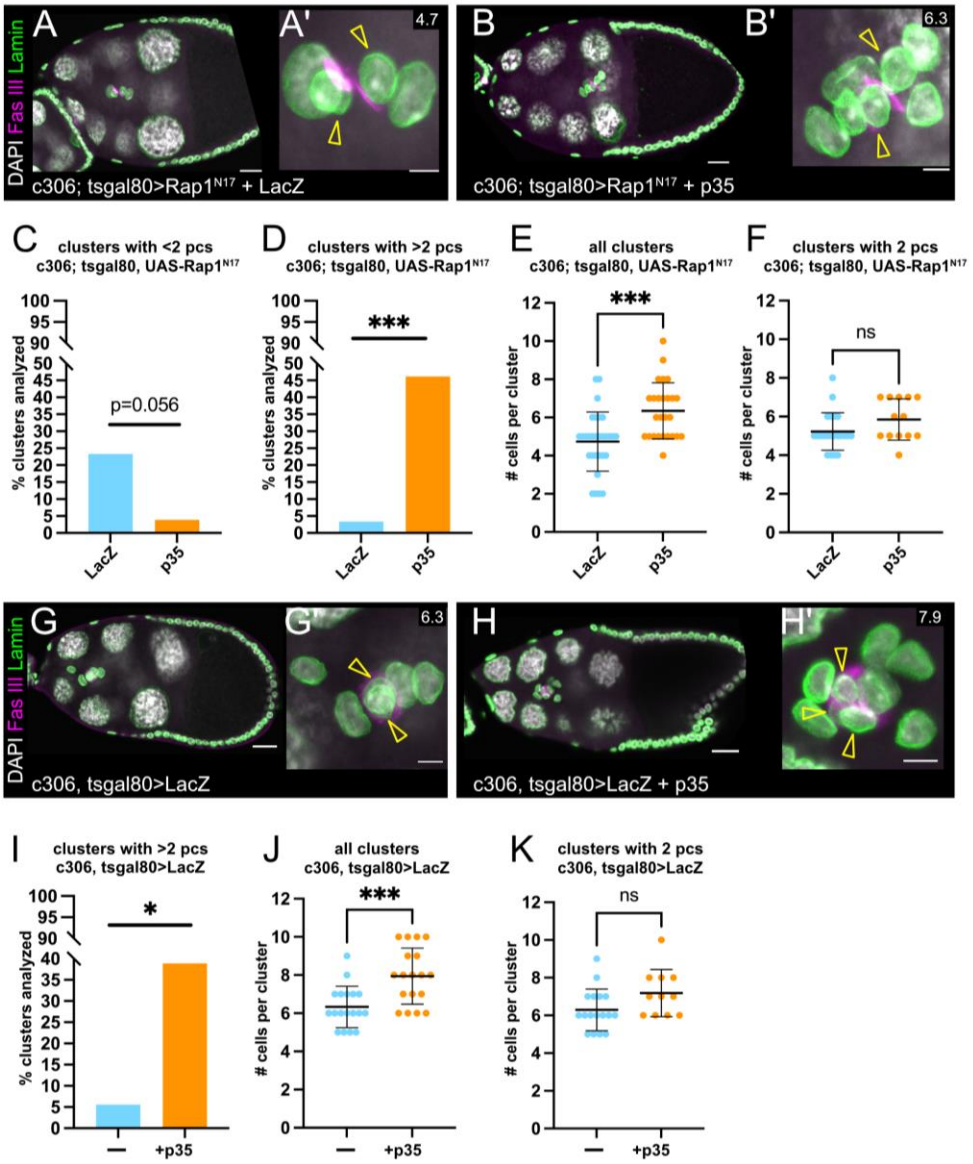

Figure 9. Inhibiting apoptosis with p35 restores cluster size and polar cell numbers

(A-B) Stage 9-10 egg chambers for DN-Rap1^{N17} + LacZ expression control (A) or DN-Rap1^{N17} + p35 (B). (A'-B') Maximum intensity projections of border cell clusters from egg chambers pictured in A and B. The numbers at the top right are the average number of cells observed for each genotype. Arrowheads indicate polar cells. (C) Quantification of border cell clusters with <2 polar cells for each genotype. p=0.056 two-sided Fisher's exact test. N≥26 border cell clusters per genotype. (D) Quantification of border cell clusters with >2 polar cells for each genotype. *** p≤0.001 two-sided Fisher's exact test. N≥26 border cell clusters per genotype. (E) Quantification of total cell number per cluster for all clusters analyzed. *** p≤0.001 two-tailed unpaired t test. N≥26 border cell clusters per genotype. (F) Quantification of total cell number

per cluster for clusters with 2 polar cells (pcs); not significant (ns), two-tailed unpaired t test. N≥13 border cell clusters per genotype. (G-H) Stage 9-10 egg chambers for LacZ alone (G) or LacZ + p35 (H). (G'-H') Close up view, maximum intensity projections of border cell clusters from egg chambers pictured in G and H. Arrowheads indicate polar cells. The numbers at the top right are the average number of cells observed for each genotype. (I) Quantification of border cell clusters with >2 polar cells for each genotype. * $p<0.05$ two-sided Fisher's exact test. N=18 border cell clusters per genotype. (J) Quantification of total cell number per cluster for all clusters analyzed. *** $p\leq0.001$ two-tailed unpaired t test. N=18 border cell clusters per genotype. (K) Quantification of total cell number per cluster for clusters with 2 pcs. ns two-tailed unpaired t test. N≥11 border cell clusters per genotype. (A, B, G, H) Scale bars 20μm. (A', B', G', H') Scale bars 5μm.

Supplemental Figures and Supplemental Figure Legends

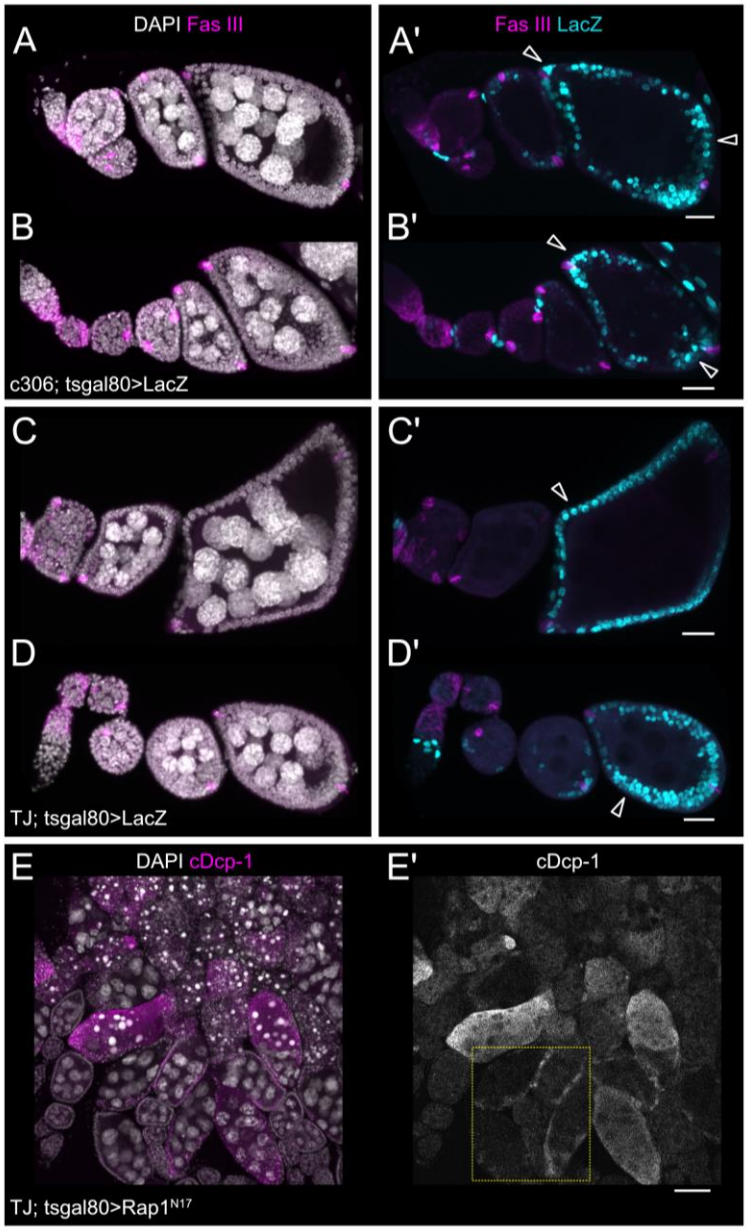

Figure S1. GAL4 expression patterns and cell death and degeneration caused by *TJ-GAL4*-driven DN-Rap1^{N17}

(A-D) Maximum intensity projections of ovarioles expressing LacZ under control of *c306-GAL4* (A-B) or *TJ-GAL4* (C-D) showing DAPI (gray) and FASIII (magenta). (A'-D') Same images as in A-D showing LacZ expression pattern (cyan) with FASIII (magenta). Arrowheads point to notable expression pattern differences. *c306-GAL4* (A', B') is expressed primarily in anterior and posterior follicle cells during oogenesis stage 7-8. *TJ-GAL4* (C', D') is expressed in all follicle

cells including those in the middle of the egg chamber at stage 7-8. (E-E') DN-Rap1^{N17} expression driven by *TJ-GAL4* causes wide-scale egg chamber death during oogenesis. DAPI (gray) and cDcp-1 (magenta) in E. Single channel image of cDcp-1 shown in E'. Yellow box indicates egg chambers that accumulate cDcp1 in follicle cells. (A'-D') Scale bars 20μm. (E') Scale bar 50μm.

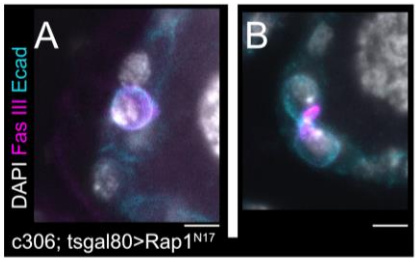

Figure S2. Rap1 inhibition causes polar cell loss and distorted polar cell shapes

(A-B) Anterior regions of two different DN-Rap1^{N17} staged 7-8 egg chambers. (A) Only one mature polar cell is present. (B) A pair of polar cells are stretched along the dorsoventral axis. Scale bars 5μm.

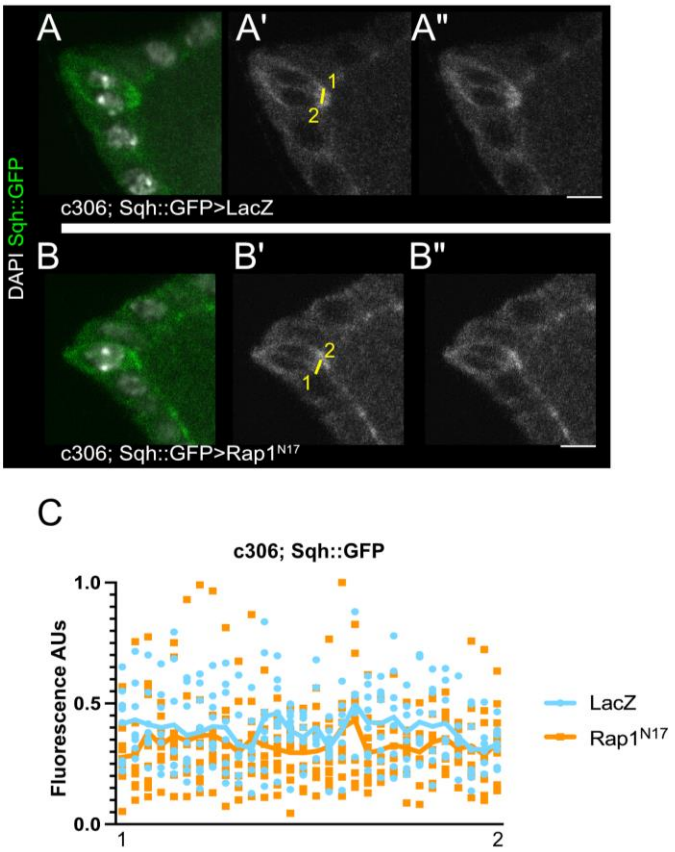

Figure S3. Rap1 is dispensable for Sqh apical localization in polar cells

(A-B) Anterior regions of stage 7-8 LacZ (A) or DN-Rap1^{N17} (B) egg chambers. (A', B') Single channel images from A and B showing Sqh::GFP (gray) with yellow lines indicating region of measurement for Sqh::GFP fluorescence intensity. The numbers correspond to the plot intensity profiles in C. (A", B") Single channel images as in A' and B' with lines removed for clarity. The image brightness was adjusted for presentation purposes but not used for quantification. (C) Profile of the intensity values along the measurement lines, plotted and scaled to the highest signal observed. The numbers on the x-axis correspond to the lines drawn on A' and B'. Solid plot lines represent the mean intensity. N ≥ 8 egg chambers per genotype. Scale bars 5μm.

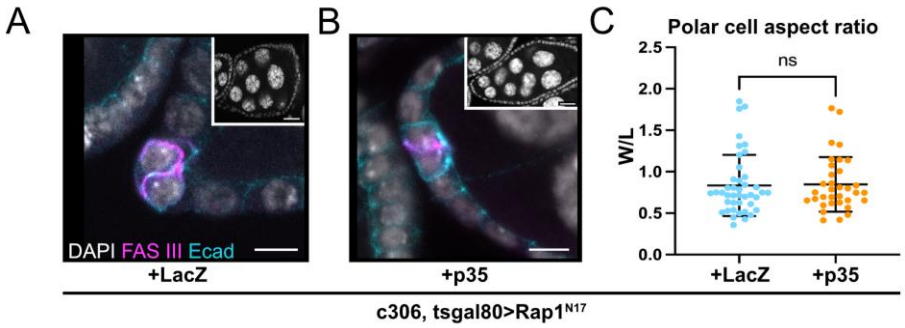

Figure S4. Rap1 promotes mature polar cell shape independent of apoptosis

(A-B) Anterior region of stage 7-8 egg chambers, DN-Rap1^{N17} with LacZ expression (A) or DN-Rap1^{N17} with apoptosis inhibitor p35 (B). Whole egg chambers stained for DAPI (gray) are shown in the insets. (C) Polar cell aspect ratio quantification. Mean AR of DN-Rap1^{N17} + LacZ control = 0.84. Mean AR of DN-Rap1^{N17} + p35 = 0.85. ns two-tailed unpaired t test. N≥34 polar cells per genotype. Main panel scale bars 5μm. Inset scale bars 20μm.

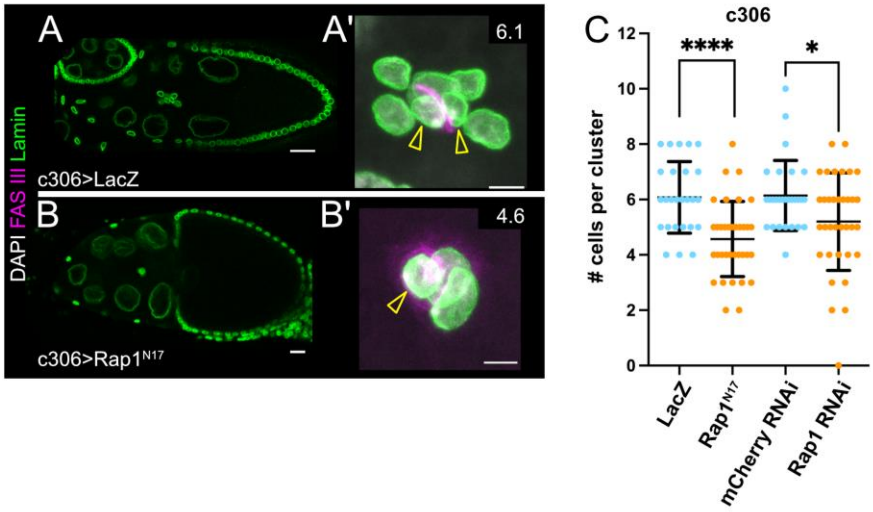

Figure S5. Rap1 is required for polar cell and border cell inclusion in migratory clusters

(A-B) Single channel Lamin images of staged 9-10 egg chambers for LacZ (A) and DN-Rap1^{N17} (B). (A'-B') Merged maximum intensity projections of border cell clusters from egg chambers pictured in A and B. The numbers at the top right are the average number of cells observed in border cell clusters for each genotype. Arrowheads indicate the polar cells. (C) Quantification of cell number per cluster for each genotype. * p≤0.05, ****p<0.0001 two-tailed unpaired t test. N≥26 border cell clusters per genotype. (A, B) Scale bars 20μm. (A', B') Scale bars 5μm.

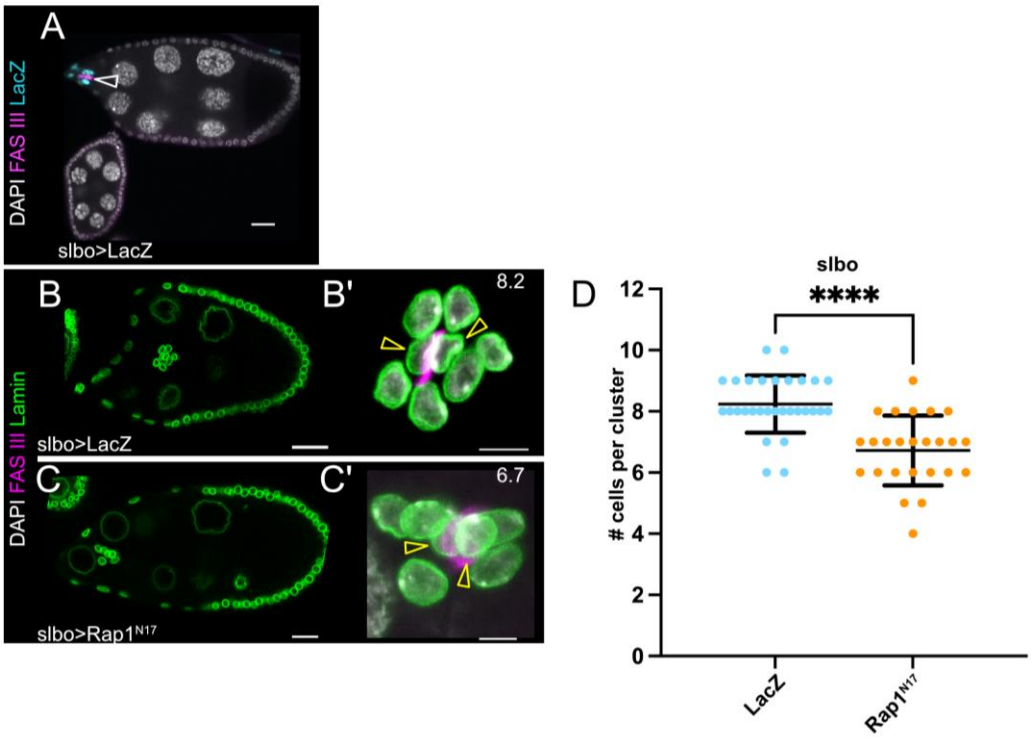

Figure S6. Effects of late Rap1 inhibition on border cell numbers

(A) Ovariole region expressing UAS-LacZ to show the expression pattern of *slbo*-GAL4 (arrowhead, GAL4-expressing cells). (B-C) Single channel Lamin (green) images of stage 9-10 LacZ (B) and DN-Rap1^{N17} (C) egg chambers showing mid-migration border cells. (B'-C') Merged maximum intensity projections of border cell clusters from B and C. Numbers in the upper right indicate the average number of cells per cluster. Arrowheads indicate polar cells (D) Quantification of cell number per cluster for Rap1 inhibition using slbo-GAL4. **** p≤0.0001 two-tailed unpaired t test. N≥25 border cell clusters per genotype. (A, B, C) Scale bars 20μm. (B', C') Scale bars 5μm.

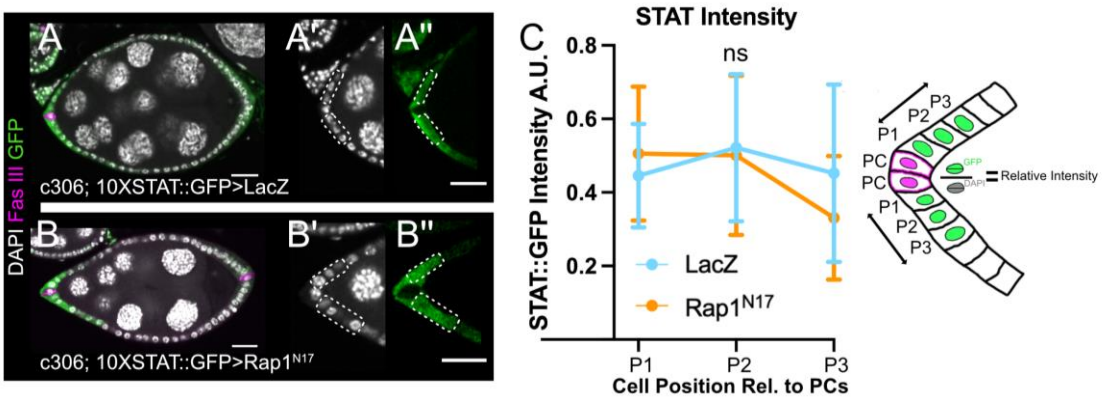

Figure S7. Rap1 is dispensable for STAT levels in follicle cells fated to become border cells

(A, B) Stage 8 LacZ (A) and DN-Rap1^{N17} (B) egg chambers with 10XSTAT::GFP reporter expression enriched adjacent to anterior polar cells. (A'-A", B'-B") Insets of the anterior end of the egg chambers in A and B, which was used to measure the intensity of nuclear 10XSTAT::GFP. (A', B') DAPI (gray). (A", B") 10XSTAT::GFP (green). Dashed rectangles indicate the cell positions next to polar cells used for analyzing STAT levels. (C) Schematic and plot of STAT intensity values relative to the DAPI signal and scaled to the highest intensity STAT measurement. ns, unpaired two-tailed t-test. N≥12 follicle cells at each position pooled from N≥6 stage 8 egg chambers for each genotype. (A, B) Scale bars 20μm. (A", B") Scale bars 5μm.

Tables

Table 1. Fly strains used in this study.

Fly Stock	Source	Used in Figures
c306-GAL4; FRT[G13], L[2]/CyO		S5
c306-GAL4, tsgal80; Sco/CyO		1, 2, 8
c306-GAL4; 10XSTAT92E-GFP	M. Starz-Gaiano	S7
c306-GAL4; UAS-Rap1N17, tsgal80	This study	9, S4
c306-GAL4; Sqh::GFP	P. Majumder from BDSC 57144	S3
c306-GAL4; tsgal80	P. Majumder	1, 2, 3, 4, 5, 6, 7, 8, S1, S2
c306-GAL4, tsgal80; LacZ/CyO	This study	9
c306-GAL4, tsgal80; PT Fas III (GFP)	This study from BDSC 50841	7
slbo-GAL4	BDSC 58435	S6
TJ-GAL4	S. Horne-Badovinac	S1
GFP-Rap1	N. Brown	1
UAS-α-Catenin RNAi	VDRC v107298	5, 6
UAS-E-Cadherin RNAi	VDRC v103962	5
UAS-GFP RNAi	VDRC v60102	5, 6
UAS-LacZ.nls	D. Montell	1, 2, 3, 4, 6, 7, 8, 9, S1, S3, S4, S5, S6, S7
UAS-mCherry RNAi	BDSC 35785	S5
UAS-p35.H	BDSC 5072	9, S4
UAS-Rap1N17	B. Boettner	1, 2, 3, 4, 6, 7, 8, S1, S2, S3, S5, S6, S7
UAS-Rap1 RNAi	VDRC v33437	S5
UAS-Rap1V12	B. Boettner	6
UAS-Sqh RNAi	VDRC v7916	5, 6

Table 2. Genotypes in this study.

Figure	Genotypes
1A	w; P[w+ GFP-Rap1]
1B	c306-GAL4/w; tsgal80/+; UAS-LacZ.nls/+
1C	c306-GAL4/w; tsgal80/+; UAS-LacZ.nls/+
1D	c306-GAL4/w; tsgal80/UAS-Rap1N17; TM2/+
1E	c306-GAL4/w; tsgal80/+; UAS-LacZ.nls/+
1F	c306-GAL4/w; tsgal80/UAS-Rap1N17; TM2/+
1G	c306-GAL4/w; tsgal80/+; UAS-LacZ.nls/+ c306-GAL4/w; tsgal80/UAS-Rap1N17; TM2/+ c306-GAL4, tsgal80/w; Sco/UAS-Rap1N17; TM2/+
2B-B"	c306-GAL4/w; tsgal80/+; UAS-LacZ.nls/+
2C-C"	c306-GAL4, tsgal80/w; Sco/UAS-Rap1N17; TM2/+
2D	c306-GAL4/w; tsgal80/+; UAS-LacZ.nls/+
2E	c306-GAL4, tsgal80/w; Sco/UAS-Rap1N17; TM2/+
2F-G	c306-GAL4/w; tsgal80/+; UAS-LacZ.nls/+ c306-GAL4, tsgal80/w; Sco/UAS-Rap1N17; TM2/+
3A-A"'	c306-GAL4/w; tsgal80/+; UAS-LacZ.nls/+
3B-B"'	c306-GAL4/w; tsgal80/UAS-Rap1N17; TM2/+
3C	c306-GAL4/w; tsgal80/+; UAS-LacZ.nls/+ c306-GAL4/w; tsgal80/UAS-Rap1N17; TM2/+
4A-A"	c306-GAL4/w; tsgal80/+; UAS-LacZ.nls/+
4B-B"	c306-GAL4/w; tsgal80/UAS-Rap1N17; TM2/+
4C-E	c306-GAL4/w; tsgal80/+; UAS-LacZ.nls/+ c306-GAL4/w; tsgal80/UAS-Rap1N17; TM2/+
5A	c306-GAL4/w; tsgal80/UAS-GFP-RNAi
5B	c306-GAL4/w; tsgal80/UAS-Sqh-RNAi
5C	c306-GAL4/w; tsgal80/UAS-E-Cadherin-RNAi
5D	c306-GAL4/w; tsgal80/UAS-α-Catenin-RNAi
5E	c306-GAL4/w; tsgal80/UAS-GFP-RNAi c306-GAL4/w; tsgal80/UAS-Sqh-RNAi c306-GAL4/w; tsgal80/UAS-E-Cadherin-RNAi c306-GAL4/w; tsgal80/UAS-α-Catenin-RNAi

5F-F'	c306-GAL4/w; tsgal80/UAS-GFP-RNAi
5G-G'	c306-GAL4/w; tsgal80/UAS-Sqh-RNAi
5H-H'	c306-GAL4/w; tsgal80/UAS-α-Catenin-RNAi
5I-I'	c306-GAL4/w; tsgal80/UAS-α-Catenin-RNAi
6A-A'	c306-GAL4/w; tsgal80/+; UAS-LacZ.nls/+
6B-B'	c306-GAL4/w; tsgal80/UAS-Rap1N17; TM2/+
6C-C'	c306-GAL4/w; tsgal80/UAS-GFP-RNAi
6D-D'	c306-GAL4/w; tsgal80/UAS-Sqh-RNAi
6E-E'	c306-GAL4/w; tsgal80/UAS-α-Catenin-RNAi
6F	c306-GAL4/w; tsgal80/+; UAS-LacZ.nls/+ c306-GAL4/w; tsgal80/UAS-Rap1N17; TM2/+ c306-GAL4/w; tsgal80/Bl; UAS-Rap1V12/+
6G	c306-GAL4/w; tsgal80/UAS-GFP-RNAi c306-GAL4/w; tsgal80/UAS-Sqh-RNAi c306-GAL4/w; tsgal80/UAS-α-Catenin-RNAi
7A-A'''	c306-GAL4/w; tsgal80/+; UAS-LacZ.nls/+
7B-B'''	c306-GAL4/w; tsgal80/UAS-Rap1N17; TM2/+
7C-C''	c306-GAL4, tsgal80/w; PT Fas III (GFP)/+; UAS-LacZ.nls/+
7D-D''	c306-GAL4, tsgal80/w; PT Fas III (GFP)/UAS-Rap1N17; TM2/+
8A-A'	c306-GAL4/w; tsgal80/+; UAS-LacZ.nls/+
8B-B'	c306-GAL4/w; tsgal80/UAS-Rap1N17; TM2/+
8C-E	c306-GAL4/w; tsgal80/+; UAS-LacZ.nls/+ c306-GAL4/w; tsgal80/UAS-Rap1N17; TM2/+
8F	c306-GAL4/w; tsgal80/+; UAS-LacZ.nls/+
8G	c306-GAL4, tsgal80/w; Sco/UAS-Rap1N17; TM2/+
8H-I	c306-GAL4/w; tsgal80/+; UAS-LacZ.nls/+. c306-GAL4, tsgal80/w; Sco/UAS-Rap1N17; TM2/+
9A-A'	c306-GAL4/w; tsgal80, UAS-Rap1N17/+; UAS-LacZ.nls/+
9B-B'	c306-GAL4/w; tsgal80, UAS-Rap1N17/UAS-p35.H
9C-F	c306-GAL4/w; tsgal80, UAS-Rap1N17/+; UAS-LacZ.nls/+ c306-GAL4/w; tsgal80, UAS-Rap1N17/UAS-p35.H
9G-G'	c306-GAL4, tsgal80/w; UAS-LacZ.nls/+
9H-H'	c306-GAL4, tsgal80/w; UAS-LacZ.nls/UAS-p35.H

9I-K	c306-GAL4, tsgal80/w; UAS-LacZ.nls/+. c306-GAL4, tsgal80/w; UAS-LacZ.nls/UAS-p35.H
S1A-A'	c306-GAL4/w; tsgal80/+; UAS-LacZ.nls/+
S1B-B'	c306-GAL4/w; tsgal80/+; UAS-LacZ.nls/+
S1C-C'	w; TJ-GAL4/+; tsgal80/UAS-LacZ.nls
S1D-D'	w; TJ-GAL4/+; tsgal80/UAS-LacZ.nls
S1E-E'	w; TJ-GAL4/UAS-Rap1N17; tsgal80/TM2
S2A-B	c306-GAL4/w; tsgal80/UAS-Rap1N17; TM2/+
S3A-A"	c306-GAL4/w; Sqh::GFP/+; UAS-LacZ.nls/+
S3B-B"	c306-GAL4/w; Sqh::GFP/UAS-Rap1N17; TM2/+
S3C	c306-GAL4/w; Sqh::GFP/+; UAS-LacZ.nls/+ c306-GAL4/w; Sqh::GFP/UAS-Rap1N17; TM2/+
S4A	c306-GAL4/w; tsgal80, UAS-Rap1N17/+; UAS-LacZ.nls/+
S4B	c306-GAL4/w; tsgal80, UAS-Rap1N17/UAS-p35.H
S4C	c306-GAL4/w; tsgal80, UAS-Rap1N17/+; UAS-LacZ.nls/+ c306-GAL4/w; tsgal80, UAS-Rap1N17/UAS-p35.H
S5A-A'	c306-GAL4/w; G13, L[2]/+; UAS-LacZ.nls/+
S5B-B'	c306-GAL4/w; G13, L[2]/UAS-Rap1N17; TM2/+
S5C	c306-GAL4/w; G13, L[2]/+; UAS-LacZ.nls/+ c306-GAL4/w; G13, L[2]/UAS-Rap1N17; TM2/+ c306-GAL4/w; G13, L[2]/+; UAS-mCherry-RNAi/+ c306-GAL4/w; G13, L[2]/+; UAS-Rap1-RNAi/+
S6A	w; slbo-GAL4/UAS-LacZ.nls
S6B-B'	w; slbo-GAL4/UAS-LacZ.nls
S6C-C'	w; UAS-Rap1N17/+; slbo-GAL4/TM2
S6D	w; slbo-GAL4/UAS-LacZ.nls w; UAS-Rap1N17/+; slbo-GAL4/TM2
S7A-A"	c306-GAL4/w; 10XSTAT92E-GFP/+; UAS-LacZ.nls/+
S7B-B"	c306-GAL4/w; 10XSTAT92E-GFP/UAS-Rap1N17; TM2/+
S7C	c306-GAL4/w; 10XSTAT92E-GFP/+; UAS-LacZ.nls/+ c306-GAL4/w; 10XSTAT92E-GFP/UAS-Rap1N17; TM2/+

Table 3. Antibodies used in this study.

Antibody	Concentration	Source	Appears in Figures
Dcp-1 (Asp215)	(1:50-1:100)	Cell Signaling Technology	6, 7, S1
DE-cadherin (DCAD2)	(1:10)	DSHB	1, 2, 3, 4, 5, 8, S2, S4
DIAP1	(1:100)	H. D. Ryoo	7
Eya (10H6)	(1:50-1:100)	DSHB	7, 8
Fas3 (7G10)	(1:5-1:10)	DSHB	3, 5, 6, 8, 9, S1, S2, S4, S5, S6, S7
GFP (12E6)	(1:10)	DSHB	1, S3
GFP (ab13970)	(1:100)	abcam	7, S7
LacZ (40-1a)	(1:10)	DSHB	1, S1, S6
Lamin (ADL67.10)	(1:10)	DSHB	9, S5, S6

Secondary antibodies used at a concentration of 1:400
Alexa Fluor Chicken 488 IgG H+L
Alexa Fluor Mouse 488 IgG H+L
Alexa Fluor Mouse 488 IgG1
Alexa Fluor Mouse 568 IgG H+L
Alexa Fluor Mouse 568 IgG2a
Alexa Fluor Rabbit 647 IgG H+L
Alexa Fluor Rat 488 IgG H+L
Alexa Fluor Rat 647 IgG H+L
DAPI (Millipore Sigma) was used at 0.05 µg/ml

Table 4. Statistics in this study.

Figure	Experimental Unit	Measurement	Experiments per Genotype (n)	Statistical Test	Significance
1G	Egg chamber	Anterior width	≥9	Unpaired two-tailed t test	ns, **
2F	Egg chamber	Cell number	≥9	Unpaired two-tailed t test	**
2G	Cell	Cell height	≥54	Unpaired two-tailed t test	***
3C	Polar cell	Aspect ratio	≥26	Unpaired two-tailed t test	ns, ****
4E	Egg chamber	Apical/Lateral E-Cad ratio	≥7	Unpaired two-tailed t test	ns
5E	Egg chamber	Anterior width	≥19	One-way ANOVA with Dunnett's Multiple Comparisons test	ns, **
6F-G	Egg chamber	cDcp+ cells	≥14	One-way ANOVA with Dunnett's Multiple Comparisons test	values in figure
8C	Border cell clusters	Polar cells	≥85	Fisher's exact test	*
8D	Border cell clusters	Cells per cluster	≥85	Unpaired two-tailed t test	****
8E	Border cell clusters	Cells per cluster	≥68	Unpaired two-tailed t test	****
8H	Egg chamber	Migration defect	≥57	Unpaired two-tailed t test	**
8I	Fly	Degenerating egg chambers	10	Unpaired two-tailed t test	ns
9C	Border cell clusters	Polar cells	≥26	Fisher's exact test	values in figure
9D	Border cell clusters	Polar cells	≥26	Fisher's exact test	***
9E	Border cell clusters	Cells per cluster	≥26	Unpaired two-tailed t test	***
9F	Border cell clusters	Cells per cluster	≥13	Unpaired two-tailed t test	ns
9I	Border cell clusters	Polar cells	18	Fisher's exact test	*

9J	Border cell clusters	Cells per cluster	18	Unpaired two-tailed t test	***
9K	Border cell clusters	Cells per cluster	≥11	Unpaired two-tailed t test	ns
S4C	Polar cell	Aspect ratio	≥34	Unpaired two-tailed t test	ns
S5C	Border cell clusters	Cells per cluster	≥26	Unpaired two-tailed t test	*, ****
S6D	Border cell clusters	Cells per cluster	≥25	Unpaired two-tailed t test	****
S7C	Nucleus	Stat reporter intensity	≥12	Unpaired two-tailed t test	ns

Significance values: * P≤0.05, ** P≤0.01, ***P≤0.001, ****P<0.0001.